

PSelInv – A Distributed Memory Parallel Algorithm for Selected Inversion : the Symmetric Case

Mathias Jacquelin, Lawrence Berkeley National Laboratory

Lin Lin, University of California, Berkeley and Lawrence Berkeley National Laboratory

Chao Yang, Lawrence Berkeley National Laboratory

We describe an efficient parallel implementation of the selected inversion algorithm for distributed memory computer systems, which we call **PSelInv**. The **PSelInv** method computes selected elements of a general sparse matrix A that can be decomposed as $A = LU$, where L is lower triangular and U is upper triangular. The implementation described in this paper focuses on the case of sparse symmetric matrices. It contains an interface that is compatible with the distributed memory parallel sparse direct factorization **SuperLU_DIST**. However, the underlying data structure and design of **PSelInv** allows it to be easily combined with other factorization routines such as **PARDISO**. We discuss general parallelization strategies such as data and task distribution schemes. In particular, we describe how to exploit the concurrency exposed by the elimination tree associated with the LU factorization of A . We demonstrate the efficiency and accuracy of **PSelInv** by presenting a number of numerical experiments. In particular, we show that **PSelInv** can run efficiently on more than 4,000 cores for a modestly sized matrix. We also demonstrate how **PSelInv** can be used to accelerate large-scale electronic structure calculations.

Categories and Subject Descriptors: G.4 [**Mathematical Software**]: —*Algorithm design and analysis*; G.4 [**Mathematical Software**]: —*Parallel and vector implementations*; I.1.2 [**Symbolic and Algebraic Manipulation**]: Algorithms—*Algebraic algorithms*

General Terms: Design, Performance

Additional Key Words and Phrases: selected inversion, sparse direct method, distributed memory parallel algorithm, high performance computation, electronic structure theory

1. INTRODUCTION

Let $A \in \mathbb{C}^{N \times N}$ be a non-singular sparse matrix. We are interested in computing *selected elements* of A^{-1} , defined as

$$\{(A^{-1})_{i,j} \mid \text{for } 1 \leq i, j \leq N, \text{ such that } A_{i,j} \neq 0\}. \quad (1)$$

Sometimes, we only need to compute a subset of these selected elements, for example, the diagonal elements of A^{-1} . The most straightforward way to obtain these selected elements of A^{-1} is to compute the full inverse of A and then extract the selected elements. But this is often prohibitively expensive in practice. It turns out that in order to compute these selected elements of A^{-1} , some additional elements of A^{-1} often need to be computed. However, the overall set of nonzero elements that need to be computed often remains a small percentage of all elements of A^{-1} due to the sparsity structure of A .

The selected elements of A^{-1} defined by (1) can be used to obtain trace estimation of the form

$$\text{Tr}[A^{-1}] \quad \text{or} \quad \text{Tr}[A^{-1}B^T], \quad (2)$$

if the sparsity pattern of $B \in \mathbb{C}^{N \times N}$ is contained in the sparsity pattern of A , i.e. $\{(i, j) | B_{i,j} \neq 0\} \subset \{(i, j) | A_{i,j} \neq 0\}$. The computation of selected elements of A^{-1} , together with the trace estimation of the form (2) arise in a number of scientific computing applications including density functional theory (DFT) [Hohenberg and Kohn 1964; Kohn and Sham 1965], dynamical mean field theory (DMFT) [Kotliar et al. 2006], Poisson-Boltzmann equation [Xu and Maggs 2013], and uncertainty quantification [Bekas et al. 2009] etc..

It is possible to compute selected elements of A^{-1} by iterative methods such as the Lanczos algorithm [Lanczos 1950; Sidje and Saad 2011], combined with Monte Carlo [Bekas et al. 2007] or deterministic probing techniques [Tang and Saad 2012]. This type of methods work well if A^{-1} is a banded matrix, or becomes a banded matrix after elements with absolute value less than ε have been truncated, and a sparse factorization of A is prohibitively expensive to perform.

In this paper we focus on using a sparse direct method to compute selected elements of A^{-1} . We assume that a sparse LU factorization (or LDL^T factorization if A is symmetric) of A is computationally feasible. The main advantage of a direct method is that we do not need to make assumptions on the decay property of A^{-1} . The disadvantage of this direct method is that it actually computes a *superset* of the selected elements of A^{-1} as defined in Eq. (1). In particular, all elements of A^{-1} indexed by the union of the nonzero index sets of the L and U factors need to be computed. It should be noted that as long as L and U remain sparse, computing elements of A^{-1} restricted to this superset can still be much faster than computing the full inverse.

Sparse direct methods for computing selected elements of A^{-1} were first proposed in the papers [Takahashi et al. 1973; Erisman and Tinney 1975]. The use of elimination tree for computing selected elements of inverse was presented in [Campbell and Davis 1995] for a sequential algorithm. Motivated by quantum transport simulations, Li et al. [Li et al. 2008; Li and Darve 2012; Li et al. 2013] developed the Fast Inverse using Nested Dissection (FIND) algorithm for computing the diagonal of A^{-1} . Some related work has recently been described in [Cauley et al. 2012; Eastwood and Wan 2013]. The FIND algorithm is in principle applicable to matrices with a general sparsity pattern, but so far its implementation focuses on structured matrices obtained from second-order partial differential operators discretized by a finite difference scheme. The implementation of FIND is not yet publicly available. Nor is it scalable to a large number of processors. [Lin et al. 2009b] developed the Hierarchically Schur Complement (HSC) method for a similar type of matrix arising from density functional theory based electronic structure calculations. The method has also been generalized and applied to quantum transport calculations [Hetmaniuk et al. 2013].

An efficient implementation of the selected inversion algorithm for a general symmetric matrix, called `SelInv`, was presented in [Lin et al. 2011b], and is publicly available. Amestoy et al. [Amestoy et al. 2012] considered a more general parallel matrix inversion method for computing any subset of entries of A^{-1} . They implemented their algorithm in the MUMPS package [Amestoy et al. 2001], which is based on the multifrontal method. In this algorithm, the actual set of computed entries of A^{-1} contains entries on the critical path of the requested entries to the root of the

elimination tree, and therefore this is also a *superset* of the requested entries of A^{-1} . This method is more efficient than our algorithm when a small number of entries of A^{-1} are requested. However, when a relatively large number of entries are to be computed such as in the computation of the selected elements defined by (1), our algorithm can reuse more efficiently the information shared among different entries of A^{-1} , and our numerical results indicate that our algorithm is more efficient than the parallel matrix inversion method implemented in MUMPS. In addition to the work presented in [Amestoy et al. 2012; Amestoy et al. 2012], parallel implementation of algorithms for computing selected elements of inverse tailored to matrices obtained from a finite difference discretization of a second-order partial differential operator have appeared in a number of publications [Petersen et al. 2009; Lin et al. 2011a]. The method developed by Petersen et al. [Petersen et al. 2009], which was designed for quasi-1D quantum transport problem, is scalable to a relatively small ($32 \sim 64$) number of processors. In [Lin et al. 2011a], we described an efficient parallel implementation for discretized 2D Laplacian type of operators, and demonstrated the efficiency of the implementation when it was used to solve a problem with billions degrees of freedom on 4,096 processors. However, this implementation cannot be used to perform a selected inversion of a general symmetric sparse matrix with an arbitrary sparsity pattern.

The purpose of this paper is to extend the selected inversion algorithm presented in [Lin et al. 2011b] and describe an implementation of a parallel selected inversion algorithm designed for distributed memory parallel computers. Such an implementation allows us to solve much larger problems by utilizing more computational resources available on high performance computers. The present work is more general than the previous work in [Lin et al. 2011a] which assumes a balanced binary elimination tree and is only applicable to structured sparse matrices obtained from finite difference discretization of differential operators. It can utilize far more number of processors than the sequential algorithm described in [Lin et al. 2011b] for general sparse matrices.

The parallel implementation of the selected inversion algorithm we present in this paper uses a more general data distribution and communication strategy to divide the work among a large number of processors to achieve multiple levels of concurrency. We name our implementation PSe1Inv and the software is publicly available. It is publicly available¹. Our first implementation focuses on the case of sparse symmetric matrices. In principle, the PSe1Inv package can be interfaced with any sparse LU and LDL^T factorization routines. Our current implementation provides an interface to the SuperLU_DIST [Li and Demmel 2003] package. The user has the option of using either the ParMETIS [Karypis and Kumar 1998] software or the PT-Scotch [Chevalier and Pellegrini 2008] package to reorder the matrix in parallel to minimize the non-zero fill in the sparse matrix factors.

The rest of the paper is organized as follows. We review the basic idea of the selected inversion method in Section 2, and discuss various implementation issues for the distributed memory parallel selected inversion algorithm in Section 3. The numerical results with applications to various matrices from including Harwell-Boeing Test Collection [Duff et al. 1992], the University of Florida Matrix Collection [Davis

¹<http://www.pexsi.org/>, distributed under the BSD license

and Hu 2011], and also applications from density functional theory are given in Section 4, followed by the conclusion and the future work discussion in Section 5.

Standard linear algebra notation is used for vectors and matrices throughout the paper. We use $A_{i,j}$ to denote the (i,j) -th entry of the matrix A , and f_i to denote the i -th entry of the vector f . With slight abuse of notation, both a supernode index and the set of column indices associated with a supernode are denoted by uppercase script letters such as $\mathcal{I}, \mathcal{J}, \mathcal{K}$ etc.. Furthermore, we use $A_{i,*}$ and $A_{*,j}$ to denote the i -th row and the j -th column of A , respectively. Similarly, $A_{\mathcal{I},*}$ and $A_{*,\mathcal{J}}$ are used to denote the \mathcal{I} -th block row and the \mathcal{J} -th block column of A , respectively. $A_{\mathcal{I},\mathcal{J}}^{-1}$ denotes the $(\mathcal{I}, \mathcal{J})$ -th block of the matrix A^{-1} , i.e. $A_{\mathcal{I},\mathcal{J}}^{-1} \equiv (A^{-1})_{\mathcal{I},\mathcal{J}}$. When the block $A_{\mathcal{I},\mathcal{J}}$ itself is invertible, its inverse is denoted by $(A_{\mathcal{I},\mathcal{J}})^{-1}$ to distinguish from $A_{\mathcal{I},\mathcal{J}}^{-1}$.

2. SELECTED INVERSION ALGORITHM

2.1 Basic formulation

Although this paper focuses on the computation of selected elements of A^{-1} when A is a sparse symmetric matrix, the idea of the selected inversion algorithm can be given for a general square matrix A , and will be used in our ongoing work for computing the selected elements of A^{-1} for asymmetric matrices. The standard approach for computing A^{-1} is to first decompose the general matrix A using the LU factorization

$$A = LU \quad (3)$$

where L is a unit lower triangular matrix and U is an upper triangular matrix. In order to stabilize the computation, matrix reordering and partial pivoting [Golub and Van Loan 1996] are usually applied to the matrix of A , and the general form of the LU factorization can be given as

$$PAQ = LU \quad (4)$$

where P and Q are two permutation matrices. To simplify the discussion below we use Eq. (3) and assume A has already been permuted.

Given the LU factorization, the most straightforward way to compute selected elements of A^{-1} is to obtain $A^{-1} \equiv (x_1, x_2, \dots, x_n)$ by solving a number of triangular systems

$$Ly_j = e_j, \quad Ux_j = y_j. \quad (5)$$

for $j = 1, 2, \dots, n$, and e_j is the j -th column of the $n \times n$ identity matrix. Such a procedure, which will be referred to as the direct inversion algorithm, is generally very costly even when A is sparse. The direct inversion algorithm performs too much computation when only a small number of selected elements of the inverse matrix are needed.

An alternative algorithm is the selected inversion algorithm, which accurately computes all the selected elements of A^{-1} . The idea of the selected inversion method originates from [Takahashi et al. 1973; Erisman and Tinney 1975], and the algorithm and its variants have been discussed in a number of recent works [Lin et al. 2009b; 2011b], [Amestoy et al. 2012; Li et al. 2008; Li and Darve 2012; Kuzmin

et al. 2013]. The selected inversion algorithm can be understood as follows. We first partition the matrix A into 2×2 blocks of the form

$$A = \begin{pmatrix} A_{1,1} & A_{1,2} \\ A_{2,1} & A_{2,2} \end{pmatrix}, \quad (6)$$

where $A_{1,1}$ is a scalar of size 1×1 . We can write $A_{1,1}$ as a product of two scalars $L_{1,1}$ and $U_{1,1}$. In particular, we can pick $L_{1,1} = 1$ and $U_{1,1} = A_{1,1}$. Then

$$A = \begin{pmatrix} L_{1,1} & 0 \\ L_{2,1} & I \end{pmatrix} \begin{pmatrix} U_{1,1} & U_{1,2} \\ 0 & S_{2,2} \end{pmatrix} \quad (7)$$

where

$$L_{2,1} = A_{2,1}(U_{1,1})^{-1}, \quad U_{1,2} = (L_{1,1})^{-1}A_{1,2}. \quad (8)$$

The L and U factors are usually directly accessible in a standard LU factorization, and

$$S_{2,2} = A_{2,2} - L_{2,1}U_{1,2} \quad (9)$$

is the Schur complement. Using the decomposition given by Eq. (7), we can express A^{-1} as

$$A^{-1} = \begin{pmatrix} (U_{1,1})^{-1}(L_{1,1})^{-1} + (U_{1,1})^{-1}U_{1,2}S_{2,2}^{-1}L_{2,1}(L_{1,1})^{-1} & -(U_{1,1})^{-1}U_{1,2}S_{2,2}^{-1} \\ -S_{2,2}^{-1}L_{2,1}(L_{1,1})^{-1} & S_{2,2}^{-1} \end{pmatrix}. \quad (10)$$

Since $S_{2,2}$ is the same as S here, without ambiguity $S_{2,2}^{-1} \equiv (S^{-1})_{2,2}$ can be used. To simplify the notation, we define the normalized LU factors as

$$\hat{L}_{1,1} = L_{1,1}, \quad \hat{U}_{1,1} = U_{1,1}, \quad \hat{L}_{2,1} = L_{2,1}(L_{1,1})^{-1}, \quad \hat{U}_{1,2} = (U_{1,1})^{-1}U_{1,2}, \quad (11)$$

and Eq. (10) can be equivalently given by

$$A^{-1} = \begin{pmatrix} (\hat{U}_{1,1})^{-1}(\hat{L}_{1,1})^{-1} + \hat{U}_{1,2}S_{2,2}^{-1}\hat{L}_{2,1} & -\hat{U}_{1,2}S_{2,2}^{-1} \\ -S_{2,2}^{-1}\hat{L}_{2,1} & S_{2,2}^{-1} \end{pmatrix}. \quad (12)$$

Let us denote by \mathcal{C} the set of indices

$$\{i | (L_{2,1})_i \neq 0\} \cup \{j | (U_{1,2})_j \neq 0\}, \quad (13)$$

and assume $S_{2,2}^{-1}$ has already been computed. From Eq. (12) it can be readily observed that in order to compute the i -th element of $A_{2,1}^{-1} \equiv -S_{2,2}^{-1}\hat{L}_{2,1}$ for $i \in \mathcal{C}$, we only need the entries

$$\left\{ (S_{2,2}^{-1})_{i,j} | i \in \mathcal{C}, j \in \mathcal{C} \right\}. \quad (14)$$

The same set of entries of $S_{2,2}^{-1}$ are required to compute selected entries of $A_{1,2}^{-1} \equiv -\hat{U}_{1,2}S_{2,2}^{-1}$. No additional entries of $S_{2,2}^{-1}$ are needed to complete the computation of $A_{1,1}^{-1}$, which involves the matrix product of selected entries of $\hat{U}_{1,2}$ and $A_{2,1}^{-1}$. This procedure can be repeated recursively to compute selected elements of $S_{2,2}^{-1}$ until $S_{2,2}$ is a scalar of size 1. A pseudo-code for demonstrating this column-based selected inversion algorithm for symmetric matrix is given in [Lin et al. 011b].

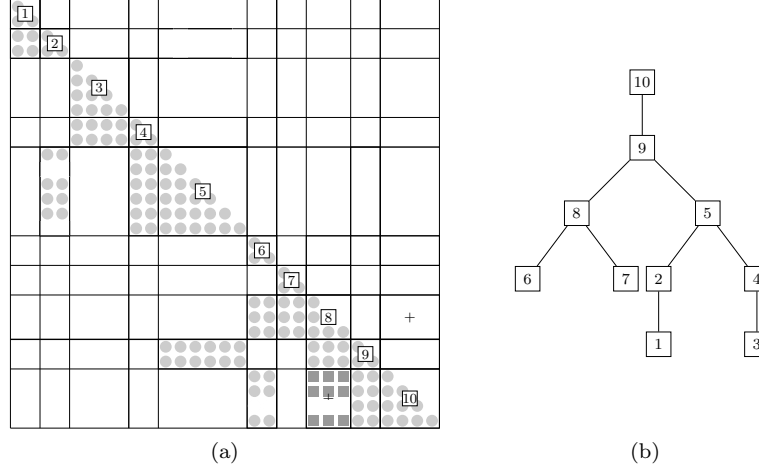


Fig. 1: (a) A structurally symmetric matrix A of size 29×29 divided into 10 supernodes. The nonzero matrix elements in A are labeled by round dots and the extra fill-in elements in L are labeled by squares. (b) The elimination tree corresponding to the matrix A and its supernode partitioning.

In practice, a column-based sparse factorization and selected inversion algorithm may not be efficient due to the lack of level 3 BLAS operations. For a sparse matrix A , the columns of A and the L factor can be partitioned into supernodes. A supernode is a maximal set of contiguous columns $\mathcal{J} = \{j, j+1, \dots, j+s\}$ of the L factor that have the same nonzero structure below the $(j+s)$ -th row, and the lower triangular part of $L_{\mathcal{J}, \mathcal{J}}$ is dense. However, this strict definition can produce supernodes that are either too large or too small, leading to memory usage, load balancing and efficiency issues. Therefore, in our work, we relax this definition to limit the maximal number of columns in a supernode (i.e. sets are not necessarily maximal). The relaxation also allows a supernode to include columns for which nonzero patterns are nearly identical to enhance the efficiency [Ashcraft and Grimes 1989]. This approach is also used in **SuperLU_DIST** [Li and Demmel 2003]. Even though the nonzero pattern of the matrix can be non-symmetric, the same supernode partitioning is usually applied to the row partition as well, and we assume the factorization has been computed using the structure of $A + A^T$. Then the nonzero structures of L and U are the transpose of each other. The total number of supernodes is denoted by \mathcal{N} . An example of the supernode partitioning of a structurally symmetric matrix A , together with the extra fill-in in its L factor (U factor omitted due to structural symmetry) are given in Fig. 1(a).

Using the notation of supernodes, a pseudo-code for the selected inversion algorithm is given in Alg. 1. The key step to gain computational efficiency in the selected inversion algorithm is step 2, which identifies the collection of all nonzero row and column indices corresponding to the supernode \mathcal{K} , denoted by \mathcal{C} . All subsequent steps operate only on these nonzero rows and columns within the sparsity pattern of the selected elements, thereby significantly reducing the computational cost.

It should be noted that if A is a sparse symmetric matrix, the normalized LU

Algorithm 1: Selected inversion algorithm based on LU factorization.

(1) The supernode partition of columns of A : $\{1, 2, \dots, \mathcal{N}\}$

Input: (2) A supernodal LU factorization of A with (unnormalized) LU factors L and U .

Output: Selected elements of A^{-1} , i.e. $A_{\mathcal{I}, \mathcal{J}}^{-1}$ such that $L_{\mathcal{I}, \mathcal{J}}$ is not an empty block.

for $\mathcal{K} = \mathcal{N}, \mathcal{N} - 1, \dots, 1$ **do**

1 Find the collection of indices
 $\mathcal{C} = \{\mathcal{I} \mid \mathcal{I} > \mathcal{K}, L_{\mathcal{I}, \mathcal{K}} \text{ is a nonzero block}\} \cup \{\mathcal{J} \mid \mathcal{J} > \mathcal{K}, U_{\mathcal{K}, \mathcal{J}} \text{ is a nonzero block}\}$

2 $\hat{L}_{\mathcal{C}, \mathcal{K}} \leftarrow L_{\mathcal{C}, \mathcal{K}}(L_{\mathcal{K}, \mathcal{K}})^{-1}, \hat{U}_{\mathcal{K}, \mathcal{C}} \leftarrow (U_{\mathcal{K}, \mathcal{K}})^{-1}U_{\mathcal{K}, \mathcal{C}}$

end

for $\mathcal{K} = \mathcal{N}, \mathcal{N} - 1, \dots, 1$ **do**

 Find the collection of indices
 $\mathcal{C} = \{\mathcal{I} \mid \mathcal{I} > \mathcal{K}, L_{\mathcal{I}, \mathcal{K}} \text{ is a nonzero block}\} \cup \{\mathcal{J} \mid \mathcal{J} > \mathcal{K}, U_{\mathcal{K}, \mathcal{J}} \text{ is a nonzero block}\}$

3 Calculate $A_{\mathcal{C}, \mathcal{K}}^{-1} \leftarrow -A_{\mathcal{C}, \mathcal{C}}^{-1} \hat{L}_{\mathcal{C}, \mathcal{K}}$

4 Calculate $A_{\mathcal{K}, \mathcal{K}}^{-1} \leftarrow U_{\mathcal{K}, \mathcal{K}}^{-1} L_{\mathcal{K}, \mathcal{K}}^{-1} - \hat{U}_{\mathcal{K}, \mathcal{C}} A_{\mathcal{C}, \mathcal{K}}^{-1}$

5 Calculate $A_{\mathcal{K}, \mathcal{C}}^{-1} \leftarrow -\hat{U}_{\mathcal{K}, \mathcal{C}} A_{\mathcal{C}, \mathcal{C}}^{-1}$

end

factors satisfy the relation

$$\hat{U}_{\mathcal{C}, \mathcal{K}} = \hat{L}_{\mathcal{K}, \mathcal{C}}^T. \quad (15)$$

To simplify the implementation, the entire diagonal block $A_{\mathcal{K}, \mathcal{K}}^{-1}$ is computed even though it is symmetric. Due to roundoff error, the numerical update in step 4 may not preserve this symmetry in finite precision. Our numerical results indicate that the loss of symmetry may accumulate, especially for ill-conditioned matrices. To reduce such error for symmetric matrices, we can simply symmetrize the diagonal block of A^{-1} by performing $A_{\mathcal{K}, \mathcal{K}}^{-1} \leftarrow \frac{1}{2} (A_{\mathcal{K}, \mathcal{K}}^{-1} + A_{\mathcal{K}, \mathcal{K}}^{-T})$ after step 4 for each \mathcal{K} .

Furthermore, it should be noted that in the symmetric case, Eq. (12) can be simplified using an LDL^T factorization which is more efficient than an LU factorization, where L is a unit lower triangular matrix, and D is a block diagonal matrix consisting of 1×1 or 2×2 blocks. The simplification of the selected inversion algorithm with an LDL^T factorization can be found in [Lin et al. 2011b]. For symmetric matrices, $A_{\mathcal{K}, \mathcal{C}}^{-1}$ (step 5) is readily obtained as the transpose of $A_{\mathcal{C}, \mathcal{K}}^{-1}$ without extra computation.

2.2 Elimination tree

Both the factorization and the selected inversion can be conveniently described in terms of traversals of an *elimination tree* [Liu 1990]. Each node of the tree corresponds to a supernode of A . A node \mathcal{R} is the parent of a node \mathcal{K} if and only if

$$\mathcal{R} = \min \{\mathcal{I} > \mathcal{J} \mid L_{\mathcal{I}, \mathcal{J}} \text{ is a nonzero block}\}. \quad (16)$$

An example of the elimination tree corresponding to the matrix in Fig. 1(a) is given in Fig. 1(b).

In the factorization procedure, the traversal of the elimination tree is a bottom-up process that starts from the leaves of the tree. A parent supernode cannot be factored until the supernodes associated with all its children in the tree have been factored. This type of task dependency also determines the amount of concurrency that can be exploited to speed up the factorization on a parallel computer.

In the selected inversion procedure, the traversal of the elimination tree is a top-down process that starts from the root of the tree. Computing the selected elements in the \mathcal{K} -th supernode of A^{-1} requires the selected elements of A^{-1} already computed at ancestor nodes of \mathcal{K} , but not those computed at its sibling nodes and their descendants. Consequently, the selected inversion of supernodes that belong to two different branches of the elimination tree can be in principle carried out independently as long as the selected elements computed at supernodes above these branches have been passed to processors that are assigned to work on these branches.

3. DISTRIBUTED MEMORY PARALLEL SELECTED INVERSION ALGORITHM

In this paper we present the distributed memory **PSelInv** method. Our first implementation focuses on the case of symmetric matrices. For such matrices, the selected inversion algorithms described in Algorithm 1 requires a sparse LU or LDL^T factorization of A to be available first. In this paper we use the **SuperLU.DIST** software package [Li and Demmel 2003] to obtain the LU factorization, which has been shown to be scalable to a large number of processors on distributed memory parallel machines. The relatively simple data structure of **SuperLU.DIST** allows easy access to sparse L and U factors. However, the main ideas we develop here can be combined with other sparse matrix solvers such as **MUMPS** [Amestoy et al. 2001] and **PARDISO** [Schenk and Gartner 2006] too, which provides the LDL^T functionality and can potentially be two times faster in the factorization phase. We also note that only symmetric permutation of the matrix A is allowed, even though **SuperLU.DIST** allows the column permutation to be different from the row permutation. In this work we do not perform equilibration procedure often used in the LU factorization to modify poorly scaled matrix elements, in order to preserve the symmetry of the matrix. In the current implementation of the **PSelInv** method, we explicitly take advantage of the symmetry of the matrix, and only compute the lower triangular part of the selected elements of A^{-1} . However, our implementation is not optimal in terms of memory allocation, in the sense that both the upper and lower triangular part of A^{-1} are stored. As will be seen below, such a strategy simplifies the communication pattern and efforts for bookkeeping in the case of 2D block cyclic data distribution, and facilitates generalizing **PSelInv** to asymmetric matrices. We also note that the sub-optimal memory allocation is not a severe limitation of the **PSelInv** method. The memory footprint of **PSelInv** can be further optimized for applications that are constrained by the memory usage. Our numerical results also indicate that the additional memory usage by **PSelInv** is relatively small compared to that used in other procedures such as the parallel numerical factorization.

We use the same 2D block cyclic distribution scheme employed in **SuperLU.DIST**

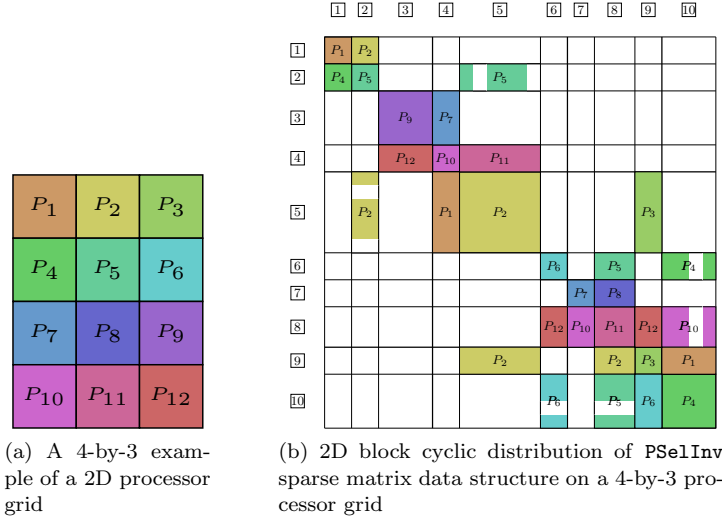


Fig. 2: Data layout of the internal sparse matrix data structure used by PSeInv.

to partition and to distribute both the L factor and the selected elements of A^{-1} to be computed. We will review the main features of this type of distribution in Section 3.1. In the 2D block cyclic distribution scheme, each supernode \mathcal{K} is assigned to and partitioned among a subset of processors. However, computing the selected elements of A^{-1} contained in the supernode \mathcal{K} requires retrieving previously computed selected elements of A^{-1} that belong to ancestors of \mathcal{K} in the elimination tree. These selected elements may reside on other processors. As a result, communication is required to transfer data among different processors to complete steps 3, 4 and 5 of Alg. 1 in each iteration. We will discuss how this is done in Section 3.2. The key to reducing communication cost and achieving scalable performance is to overlap communication with computation by using asynchronous point-to-point MPI functions, even though some of these communication events are collective in nature (e.g., broadcast and reduce) within a communication subgroup.

In addition to utilizing a fine grain level of parallelism in computing A^{-1} for each supernode, we introduce a coarse grain level of parallelism by exploiting the concurrency available in the elimination tree. This amounts to executing different iterates of the for loop in Alg. 1 in parallel. Although the elimination tree may exhibit many independent tasks associated with supernodes that belong to different branches of the elimination tree, the 2D block cyclic distribution of L and A^{-1} may prevent these tasks from being performed completely simultaneously on different processors. The key to minimizing the dependency issue is to properly assign the order of computational tasks, and to overlap computation and communication as much as possible. We will discuss our preliminary strategy for improving the parallel efficiency using elimination tree in Section 3.3.

3.1 Distributed data layout and structure

As discussed in Section 2, the columns of A , L and U are partitioned into supernodes. Different supernodes may have different sizes. The same partition is applied

to the rows of these matrices to create a 2D block partition of these matrices. The submatrix blocks are mapped to processors that are arranged in a virtual 2D grid of dimension $P_r \times P_c$ in a cyclic fashion as follows: The $(\mathcal{I}, \mathcal{J})$ -th matrix block is held by the processor labeled by

$$P_{\text{mod}(\mathcal{I}-1, P_r) \times P_c + \text{mod}(\mathcal{J}-1, P_c) + 1}. \quad (17)$$

This is called a 2D block cyclic data-to-processor mapping. The mapping itself does not take the sparsity of the matrix into account. If the $(\mathcal{I}, \mathcal{J})$ -th block contains only zero elements, then that block is not stored. It is possible that some nonzero blocks may contain several rows of zeros. These rows are not stored either. As an example, a 4-by-3 grid of processors is depicted in Fig. 2(a). The mapping between the 2D supernode partition of the matrix in Fig. 1(a) and the 2D processor grid in Fig. 2(a) is depicted in Fig. 2(b). Each supernodal block column of L is distributed among processors that belong to a column of the processor grid. Each processor may own multiple matrix blocks. For instance, the nonzero rows in the second supernode are owned by processors P_2 and P_5 . More precisely, P_2 owns two nonzero blocks, while P_5 is responsible for one block. Note that these nonzero blocks are not necessarily contiguous in the global matrix. Though the nonzero structure of A is not taken into account during the distribution, it has been shown in practice that 2D layouts leads to higher scalability for both dense [Blackford 1997], sparse Cholesky factorizations [Rothberg and Gupta 1994] and LU factorization [Li and Demmel 2003].

In the current implementation, `PSelInv` contains an interface that is compatible with the `SuperLU_DIST` software package. In order to allow `PSelInv` to be easily integrated with other LDL^T or LU factorization codes, we create some intermediate sparse matrix objects to hold the distributed L and U factors. Such intermediate sparse matrix objects will be overwritten by selected elements of A^{-1} in the selected inversion process. Each nonzero block $L_{\mathcal{I}, \mathcal{J}}$ is stored as follows. Diagonal blocks $L_{\mathcal{I}, \mathcal{I}}$ are always stored as dense matrices. Nonzero entries of $L_{\mathcal{I}, \mathcal{J}}$ ($\mathcal{I} > \mathcal{J}$) are stored contiguously as a dense matrix in a column-major order even though row indices associated with the stored matrix elements are not required to be contiguous. As mentioned at the beginning of Section 3, our implementation is not optimal in terms of memory allocation for symmetric matrices, in the sense that the nonzero entries of within $U_{\mathcal{I}, \mathcal{J}}$ ($\mathcal{I} < \mathcal{J}$) are also stored as a dense matrix in a contiguous array in a column major order, even though the values of $U_{\mathcal{I}, \mathcal{J}}$ are identical to those of $L_{\mathcal{J}, \mathcal{I}}^T$ for symmetric matrices. The nonzero column indices associated with the nonzeros entries in $U_{\mathcal{I}, \mathcal{J}}$ are not required to be contiguous either. We remark that for matrices with highly asymmetric sparsity patterns, it is more efficient to store the upper triangular blocks using the skyline structure shown in [Li and Demmel 2003]. However, we choose to use a simpler data layout because it allows level-3 BLAS (GEMM) to be used in the selected inversion process.

3.2 Computing selected elements of A^{-1} within each supernode in parallel

In this section, we detail how steps 2 to 5 in Alg. 1 can be completed in parallel.

We perform step 2 of Alg. 1 in a separate pass, since the data communication required in this step is relatively simple. The processor that owns the block $L_{\mathcal{K}, \mathcal{K}}$ broadcasts $L_{\mathcal{K}, \mathcal{K}}$ to all other processors within the same column processor group

owning nonzero blocks $L_{\mathcal{I},\mathcal{K}}$ in the supernode \mathcal{K} . Each processor in that group performs the triangular solve $\hat{L}_{\mathcal{I},\mathcal{K}} \equiv L_{\mathcal{I},\mathcal{K}}(L_{\mathcal{K},\mathcal{K}})^{-1}$ for each nonzero block contained in the set \mathcal{C} defined in step 1 of the algorithm. Because $L_{\mathcal{I},\mathcal{K}}$ is not used in the subsequent steps of selected inversion once $\hat{L}_{\mathcal{I},\mathcal{K}}$ has been computed, it is overwritten by $\hat{L}_{\mathcal{I},\mathcal{K}}$. Since communication is limited to a processor column group only, step 2 can be carried out for multiple supernodes at the same time.

A more complicated communication pattern is required to complete step 3 in parallel. Because $A_{\mathcal{C},\mathcal{C}}^{-1}$ and $\hat{L}_{\mathcal{C},\mathcal{K}}$ are generally owned by different processor groups, there are two possible ways to carry out the multiplication of $A_{\mathcal{C},\mathcal{C}}^{-1}$ with $\hat{L}_{\mathcal{C},\mathcal{K}}$. The first approach is to send blocks of $\hat{L}_{\mathcal{C},\mathcal{K}}$ to processors that own the *matching* blocks of $A_{\mathcal{C},\mathcal{C}}^{-1}$, so that matrix-matrix multiplication can be performed on processors owning $A_{\mathcal{C},\mathcal{C}}^{-1}$. The second approach is to send data in the opposite direction, *i.e.* one can send blocks of $A_{\mathcal{C},\mathcal{C}}^{-1}$ to the *matching* blocks of $\hat{L}_{\mathcal{C},\mathcal{K}}$, so that matrix-matrix multiplication can be performed on processors owning $\hat{L}_{\mathcal{C},\mathcal{K}}$.

In order to compare the cost of these two approaches, let us first consider the case in which all blocks $\hat{L}_{\mathcal{I},\mathcal{K}}$ with $\mathcal{I} \geq \mathcal{K}$ are dense matrix blocks of equal size $m_b \times m_b$, and $\mathcal{C} = \{\mathcal{I} | \mathcal{I} \geq \mathcal{K}\}$. This is approximately the case when \mathcal{K} is near the root of the elimination tree. We assume that there are $\sqrt{P} \times \sqrt{P}$ processors, thus the size of the set \mathcal{C} is $m_b \sqrt{P}$. We also assume that the matrix blocks in $\hat{L}_{\mathcal{C},\mathcal{K}}$ are distributed among \sqrt{P} processors within the same column group, and each processor in this processor column also holds a dense block $\hat{L}_{\mathcal{I},\mathcal{K}}$ of size $m_b \times m_b$. In the first approach, the computation is performed in parallel on P processors, and the computational cost on each processor is $\mathcal{O}(m_b^3)$. In the second approach, the computation is performed in parallel on \sqrt{P} processors only, and the computational cost on these processors is $\mathcal{O}(m_b^3 \sqrt{P})$. All other processors are idle in the computational step, and this leads to severe load imbalance when P is large.

We implemented the first approach in PSelInv. This requires sending the $\hat{L}_{\mathcal{I},\mathcal{K}}$ block from a particular processor to all processors within the same column group of processors among which $A_{\mathcal{C},\mathcal{I}}^{-1}$ is distributed. However, since the processor owning $\hat{L}_{\mathcal{I},\mathcal{K}}$ is generally not in the same processor communication group that owns $A_{\mathcal{C},\mathcal{I}}^{-1}$, sending $\hat{L}_{\mathcal{I},\mathcal{K}}$ to processors that hold the distributed blocks of $A_{\mathcal{C},\mathcal{I}}^{-1}$ cannot be done by a single broadcast. Indeed, for this to be possible, communication groups (*i.e.* MPI communicators) would have to be created for each and every different sparse row/column structure. This is generally not possible as the maximum number of allowed MPI communicators is typically much smaller than needed. Therefore, one way to complete this step of data communication is to use a number of point-to-point MPI sends that originate from the processor that owns $\hat{L}_{\mathcal{I},\mathcal{K}}$ and terminate on the group of processors that own the nonzero blocks of $A_{\mathcal{C},\mathcal{I}}^{-1}$. In addition to incurring higher communication latency cost, this approach also leads to significant bookkeeping effort in order to track the sources and destinations of all messages for each processor.

In our current implementation, we simplify the data communication pattern by storing both $\hat{L}_{\mathcal{I},\mathcal{K}}$ and $\hat{U}_{\mathcal{K},\mathcal{I}}$ even when A is symmetric. We acknowledge that such implementation is not optimal in terms of memory allocation, and can be improved

if applications are constrained by memory usage for symmetric matrices. As soon as $\hat{L}_{\mathcal{I},\mathcal{K}}$ becomes available as illustrated above, we send the $\hat{L}_{\mathcal{I},\mathcal{K}}$ block to the processor that owns $\hat{U}_{\mathcal{K},\mathcal{I}}$, and $\hat{U}_{\mathcal{K},\mathcal{I}}$ is overwritten by $\hat{L}_{\mathcal{I},\mathcal{K}}^T$. Fig. 3 illustrates how this step is carried out for a specific supernode $\mathcal{K} = \boxed{6}$ of the matrix described in Fig. 2(b). Once $\hat{L}_{8,6}$ is computed on P_{12} , the block is sent to P_5 . The P_5 processor then overwrites $\hat{U}_{6,8}$ by $\hat{L}_{8,6}^T$. Similarly, the $\hat{L}_{10,6}$ block is computed on P_6 and sent to P_4 on which $\hat{U}_{6,10}$ is overwritten by $\hat{L}_{10,6}$.

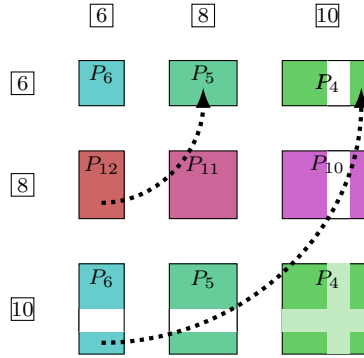


Fig. 3: Processors holding $\hat{L}_{8,6}$ and $\hat{L}_{10,6}$ send data to processors holding the cross-diagonal blocks and overwrite $\hat{U}_{6,8}$ and $\hat{U}_{6,10}$.

With $\hat{L}_{\mathcal{I},\mathcal{K}}$ properly placed on the processors that are mapped to the upper triangular part of the distributed \hat{U} matrix, step 3 of Alg. 1 can proceed as follows. The $\hat{U}_{\mathcal{K},\mathcal{I}} = \hat{L}_{\mathcal{I},\mathcal{K}}^T$ block is first sent to all processors within the same column processor group that owns $\hat{U}_{\mathcal{K},\mathcal{I}}$. The matrix-matrix multiplication $A_{\mathcal{J},\mathcal{I}}^{-1} \hat{L}_{\mathcal{I},\mathcal{K}}$ is then performed locally on each processor owning $A_{\mathcal{J},\mathcal{I}}^{-1}$ using the GEMM subroutine in BLAS3. Then local matrix contributions $A_{\mathcal{J},\mathcal{I}}^{-1} \hat{L}_{\mathcal{I},\mathcal{K}}$ are reduced within each row communication groups owning $\hat{L}_{\mathcal{J},\mathcal{K}}$ to produce the $A_{\mathcal{J},\mathcal{K}}^{-1}$ block in step 3 of Alg. 1.

Fig. 4 illustrates how this step is completed for a specific supernode $\mathcal{K} = \boxed{6}$, for the matrix depicted in Fig. 2(b). We use circled letters (a), (b), (c) to label communication events, and circled numbers (1), (2), (3) to label computational events. We can see from this figure that $\hat{U}_{6,8} = \hat{L}_{8,6}^T$ is sent by P_5 to all processors within the same column processor group to which P_5 belongs. This group include both P_5 and P_{11} . Similarly $\hat{L}_{10,6}$ is broadcast from P_4 to all other processors within the same column group to which P_4 belongs. Local matrix matrix multiplications are then performed on P_{11} , P_{10} , P_4 and P_5 simultaneously. The distributed products are then reduced onto P_{12} and P_5 within the row processor groups they belong to respectively. After this step, $A_{8,6}^{-1}$ and $A_{10,6}^{-1}$ become available on P_{12} and P_6 respectively.

Upon the completion of step 3, the matrix product $\hat{U}_{\mathcal{K},\mathcal{J}} A_{\mathcal{J},\mathcal{K}}^{-1} \equiv \hat{L}_{\mathcal{J},\mathcal{K}}^T A_{\mathcal{J},\mathcal{K}}^{-1}$ is first computed locally on the processor holding $\hat{L}_{\mathcal{J},\mathcal{K}}$, and then reduced to the processor that owns the diagonal block $L_{\mathcal{K},\mathcal{K}}$ within the column processor group

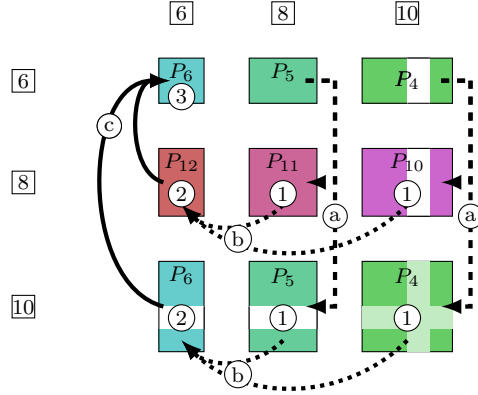


Fig. 4: Task parallelism and communication pattern for the supernode $\boxed{6}$. There are 6 steps: (a) broadcast \hat{L} , (1) compute $A^{-1}\hat{L}$, (b) reduce $A^{-1}\hat{L}$, (2) compute $\hat{L}^T A^{-1}\hat{L}$, (c) reduce $\hat{L}^T A^{-1}\hat{L}$ and (3) update A^{-1} .

that the supernode \mathcal{K} is mapped to. The sum of the distributed matrix product $-\hat{L}_{\mathcal{J},\mathcal{K}}^T A_{\mathcal{J},\mathcal{K}}^{-1}$ is then added to $(U_{\mathcal{K},\mathcal{K}})^{-1}(L_{\mathcal{K},\mathcal{K}})^{-1}$ computed on the processor holding $L_{\mathcal{K},\mathcal{K}}$. This completes step 4 of Alg. 1. As an example we use again Fig. 4 for $\mathcal{K} = \boxed{6}$. $\hat{L}_{8,6}^T A_{8,6}^{-1}$ is computed on P_{12} and sent to P_6 . Similarly $\hat{L}_{10,6}^T A_{10,6}^{-1}$ is computed on P_6 . Since both $\hat{L}_{10,6}^T$ and $L_{6,6}$ are held by P_6 , no further data communication is necessary. Finally P_6 updates $A_{6,6}^{-1}$. As we discussed in Section 2.1, for symmetric matrices, $A_{\mathcal{K},\mathcal{K}}^{-1}$ should be explicitly symmetrized to reduce the effect of rounding errors.

Since A is symmetric, step 5 of Alg. 1 can be simplified as follows. We first overwrite $\hat{L}_{\mathcal{J},\mathcal{K}}$ by $A_{\mathcal{J},\mathcal{K}}^{-1}$ locally on the processor holding $\hat{L}_{\mathcal{J},\mathcal{K}}$ ($\mathcal{J} > \mathcal{K}$). We then send $A_{\mathcal{J},\mathcal{K}}^{-1}$ to the processor holding $\hat{U}_{\mathcal{K},\mathcal{J}}$, and overwrite $\hat{U}_{\mathcal{K},\mathcal{J}}$ by $(A_{\mathcal{J},\mathcal{K}}^{-1})^T$. The data communication pattern for this step is the same as described in Fig. 3. After step 5 we move to the next supernode ($\mathcal{K} - 1$).

3.3 Exploiting concurrency in the elimination tree

In this section, we discuss how to add an additional coarse-grained level of parallelism to the selected inversion algorithm by exploiting task concurrency exposed by the elimination tree.

As we indicated in Section 2.2, two supernodes belonging to two separate branches of the elimination tree can be processed independently if the selected elements of the inverse belonging to their ancestors have been computed, and if these supernodes and the ancestors they depend on are mapped onto different sets of processors. Although it is possible to pass the previously computed selected elements of A^{-1} from the ancestors down to their children as we move down the elimination tree, algorithms based on this approach (e.g., a multifrontal like algorithm [Lin et al. 011a]) would require additional work space to hold extra copies of the selected elements.

To reduce the amount of extra work space, which can grow rapidly as we go down

the elimination tree, we choose to allow processors assigned to each supernode to communicate back and forth with processors assigned to its ancestors in the way that we described in Section 3.2 to complete step 3 of Alg. 1.

However, the drawback of this approach is that, at some point, two supernodes belonging to two separate branches of the elimination tree may not be processed simultaneously when they need to communicate with their common ancestors at the same time. At this point of conflict, only one of them should be allowed to initiate and complete the data communication with the common ancestor at a time. For example, when supernodes [2] and [4] in Fig. 1(a) are being processed on different sets of processors, both of them may need to communicate with processors assigned to supernode [5] at the same time. In this case, the updates to be performed on these processors cannot proceed completely independently. On the other hand, if the set of processors assigned to update two supernodes are completely different, then at least some of the updates can be computed simultaneously.

In order to exploit the type of concurrency discussed above, which occurs at the **for** loop level in Alg. 1, we create a basic parallel task scheduler to launch different iterates of the **for** loop in a certain order. This order is defined by a priority list S , which is indexed by integer priority numbers ranging from 1 to n_s , where n_s is bounded from above by the depth of the elimination tree. The task performed in each iteration of the **for** loop is assigned a priority number $\sigma(\mathcal{I})$. The lower the number, the higher the priority of the task, hence the sooner it is scheduled. The supernode \mathcal{N} associated with the root of the elimination tree clearly has to be processed first. If the k -th element of S contains multiple supernodes or tasks whose priority numbers are k , the order in which these tasks are completed can be arbitrary. A recipe for assigning priority number of different tasks (or equivalently, supernodes) is shown in Alg. 2. We assume that the elimination tree is post-ordered.

Even though we use a priority list to help launch tasks, we do not place extra synchronization among launched tasks other than requiring them to preserve data dependency. Tasks associated with different supernodes can be executed concurrently if these supernodes are on different critical paths of the elimination tree, and if there is no overlap among processors mapped to these critical paths. In fact, if tasks associated with supernode \mathcal{J} and \mathcal{I} are mapped to different sets of processors, the task associated with the supernode \mathcal{J} may actually start before that associated with another supernode \mathcal{I} even if $\sigma(\mathcal{I}) < \sigma(\mathcal{J})$, i.e. even if task \mathcal{I} is scheduled ahead of task \mathcal{J} according to the priority list. When two different tasks need to communicate with a common ancestor, the priority number associated with each task determines which task is completed first.

We remark that there is some flexibility in assigning a priority number to each supernode and constructing the priority list S . For instance, we can use the strategy given by Alg. 2, which simply defines $\sigma(\mathcal{I})$ by the distance (in terms of the number of edges) between the supernode \mathcal{I} and the root of the elimination tree. For the same elimination tree shown in Fig. 5(a), another possible construction of the σ list is illustrated in Fig. 5(b), which assigns the same σ value to supernodes at different levels of the elimination tree. The latter construction takes into account how supernodes are distributed among different processors as we will discuss below.

The priority list S determines the order in which computational tasks associated

Algorithm 2: Assign priority numbers to supernodes and create a priority list.

Input: a list of supernodes $\{\mathcal{I}\}$ and the elimination tree associated with these supernodes.

Output: an array σ , $\sigma(\mathcal{I})$ gives the priority number of the task associated with supernode \mathcal{I} ; an array S of n_s supernode lists, $S(i)$ gives a set of supernodes with priority number i , $1 \leq i \leq n_s$.

```

 $\sigma(\mathcal{N}) = 1$ 
 $S(1) = \{\mathcal{N}\}$ 
for  $\mathcal{I} = \mathcal{N} - 1$  down to 1 do
    |  $\sigma(\mathcal{I}) = \sigma(\text{parent}(\mathcal{I})) + 1$ 
    |  $S(\sigma(\mathcal{I})) = S(\sigma(\mathcal{I})) \cup \{\mathcal{I}\}$ 
end
    
```

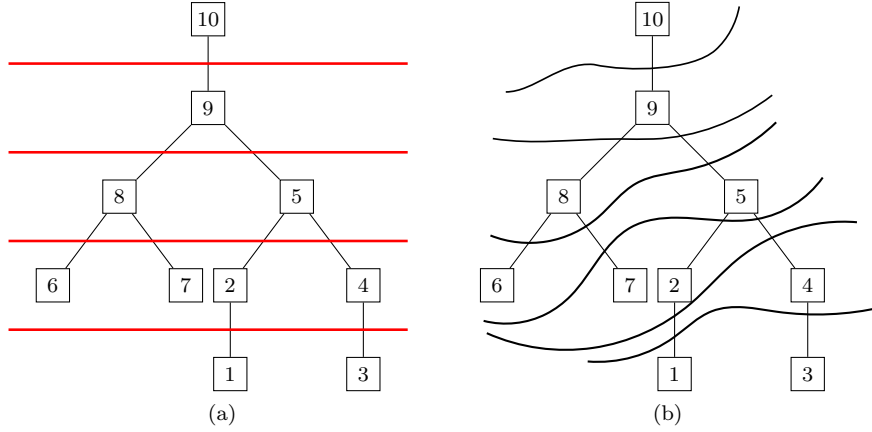


Fig. 5: Elimination tree of matrix A and two possible priority lists S .

with different supernodes are completed. Because the amount of work and communication performed by each supernodes can vary significantly, different priority lists can lead to different overall performance. The actual performance of parallel selected inversion depends on the sparsity pattern of the matrix as well as the processor grid, and is therefore difficult to predict *a priori*. We refer readers to our report [Jacquelin et al. 2014] for a detailed example on the difficulty of designing an optimal task schedule.

With the help of the priority list, we can implement the **for** loop level of parallelism in Alg. 1 in a way that is described in Alg. 3. To illustrate the relation clearly, Alg. 3 uses the same numeric ordering of the steps as that in Alg. 1. Alg. 3 also makes use of another array of lists **procmap**. The \mathcal{K} -th element of **procmap** contains the list of all processors participating in steps 3 – 5 in Alg. 1. The communication steps are described within parentheses. We also remark that we do not place MPI barriers between supernodes explicitly to exploit parallelism among the computation for different supernodes. For symmetric matrices, the diagonal blocks

should be symmetrized, as indicated at the end of Section 2.1 for symmetric cases.

4. NUMERICAL RESULTS

To assess the performance of **PSe1Inv**, we conducted a number of computational experiments which we report in this section.

Our test problems are taken from various sources including Harwell-Boeing Test Collection [Duff et al. 1992], the University of Florida Matrix Collection [Davis and Hu 2011], and matrices generated from electronic structure software including SIESTA [Soler et al. 2002] and DGDFT [Lin et al. 2012]. The first two matrix collections are widely used benchmark problems for testing sparse direct methods, while the other test problems come from practical large scale electronic structure calculations. The names of these matrices as well as some of their characteristics are listed in Tables I and II. The first three problems in these tables come with two matrices each. One of the matrices, denoted by H , is a discretized Hamiltonian, and the other matrix is an overlap matrix denoted by S . For all other problems, the overlap matrices can be considered as the identity matrix. All matrices are real and symmetric. In all our experiments, we compute the selected elements of the matrix

$$A(z) = H - zS. \quad (18)$$

For simplicity, we choose $z = 0$ for all the efficiency tests in Section 4.1. For some applications, z is chosen to be a complex number with a small imaginary part to ensure that $A(z)$ is nonsingular. This technique is often used in electronic structure calculation to be discussed in Section 4.3. The LU factorization is performed by using the **SuperLU_DIST** software package. **SuperLU_DIST** does not use dynamic pivoting strategies and our matrices are permuted without taking into account the values of matrix entries. Consequently the efficiency of both **SuperLU_DIST** and **PSe1Inv** is independent of the choice of z . The lack of dynamic pivoting strategies may impact the accuracy of **PSe1Inv** for highly indefinite and nearly singular systems. We study the accuracy for different choices of complex shifts z in Section 4.2. All the timing results reported are performed in complex arithmetic computation.

In all of our experiments, we used the NERSC Edison platform with Cray XC30 nodes. Each node has 24 cores partitioned among two Intel Ivy Bridge processors. Each 12-core processor runs at 2.4GHz. A single node has 64GB of memory, providing more than 2.6 GB of memory per core. We used one MPI process per core, and refer to core to denote an MPI process.

4.1 Parallelization scalability

Four types of experiments were performed to measure the scalability of **PSe1Inv**. For the first three sets of experiments, all the timing data points we present are averaged measurements over 10 runs, and the error bars shown in Figures 6, 7, 8 and 9 indicate the standard deviation of the measured wall clock time.

In order to clearly show the cost and scalability of selected inversion itself in comparison with the symbolic and numerical LU factorizations, which are required for selected inversion, we time the three computational components separately. The symbolic factorization is performed in parallel using **PT-Scotch**. It is labeled by

Algorithm 3: The parallel selected inversion algorithm (for symmetric matrices).

Input:

- (1) The supernode partition of columns of a sparse symmetric matrix A : $\{1, 2, \dots, \mathcal{N}\}$; a priority list $\{S(k)\}$: $k = 1, 2, \dots, n_s$;
- (2) L and U factors through a supernodal LU factorization (or equivalent LDL^T factorization) of A ;
- (3) 2D processor mapping with $P = \text{Pr} \times \text{Pc}$ processors.

Output: Selected elements of A^{-1} .

[Compute the normalized factors \hat{L} and \hat{U}].

for $k = 1, 2, \dots, n_s$ **do**

for each supernode $\mathcal{K} \in S(k)$ **do**

if $\text{myid} \in \text{procmap}(\mathcal{K})$ **then**

1 Find the collection of indices $\mathcal{C} = \{\mathcal{I} \mid \mathcal{I} >$
 $\mathcal{K}, L_{\mathcal{I}, \mathcal{K}} \text{ is a nonzero block}\} \cup \{\mathcal{J} \mid \mathcal{J} > \mathcal{K}, U_{\mathcal{K}, \mathcal{J}} \text{ is a nonzero block}\}$
2 (Broadcast $(L_{\mathcal{K}, \mathcal{K}})^{-1}$ to processors owning $L_{\mathcal{I}, \mathcal{K}}, \mathcal{I} \in \mathcal{C}$)
2 $\hat{L}_{\mathcal{C}, \mathcal{K}} \leftarrow L_{\mathcal{C}, \mathcal{K}}(L_{\mathcal{K}, \mathcal{K}})^{-1}$
2 (Send $\hat{L}_{\mathcal{I}, \mathcal{K}}, \mathcal{I} \in \mathcal{C}$ to the processor holding $\hat{U}_{\mathcal{K}, \mathcal{I}}, \mathcal{I} \in \mathcal{C}$ and
 overwrite $\hat{U}_{\mathcal{K}, \mathcal{I}}, \mathcal{I} \in \mathcal{C}$ by $\hat{L}_{\mathcal{I}, \mathcal{K}}^T, \mathcal{I} \in \mathcal{C}$)

end

end

end

[Selected inversion process].

for $k = 1, 2, \dots, n_s$ **do**

for each supernode $\mathcal{K} \in S(k)$ **do**

if $\text{myid} \in \text{procmap}(\mathcal{K})$ **then**

 Find the collection of indices $\mathcal{C} = \{\mathcal{I} \mid \mathcal{I} >$
 $\mathcal{K}, L_{\mathcal{I}, \mathcal{K}} \text{ is a nonzero block}\} \cup \{\mathcal{J} \mid \mathcal{J} > \mathcal{K}, U_{\mathcal{K}, \mathcal{J}} \text{ is a nonzero block}\}$
3 (Broadcast $\hat{U}_{\mathcal{K}, \mathcal{I}}, \mathcal{I} \in \mathcal{C}$ to processors holding $A_{\mathcal{J}, \mathcal{I}}^{-1}, \mathcal{I}, \mathcal{J} \in \mathcal{C}$)
3 For processors holding $A_{\mathcal{J}, \mathcal{I}}^{-1}, \mathcal{I}, \mathcal{J} \in \mathcal{C}$, compute locally
 $-A_{\mathcal{J}, \mathcal{I}}^{-1} \hat{L}_{\mathcal{I}, \mathcal{K}}, \mathcal{I}, \mathcal{J} \in \mathcal{C}$
3 (Reduce $-A_{\mathcal{J}, \mathcal{I}}^{-1} \hat{L}_{\mathcal{I}, \mathcal{K}}, \mathcal{I}, \mathcal{J} \in \mathcal{C}$ to processors holding $\hat{L}_{\mathcal{J}, \mathcal{K}}, \mathcal{J} \in \mathcal{C}$,
 and save the result in $A_{\mathcal{J}, \mathcal{K}}^{-1}, \mathcal{J} \in \mathcal{C}$)
4 For processors holding $\hat{L}_{\mathcal{I}, \mathcal{K}}, \mathcal{I} \in \mathcal{C}$, compute locally
 $-\hat{L}_{\mathcal{I}, \mathcal{K}}^T A_{\mathcal{I}, \mathcal{K}}^{-1}, \mathcal{I} \in \mathcal{C}$
4 (Reduce $-\hat{L}_{\mathcal{I}, \mathcal{K}}^T A_{\mathcal{I}, \mathcal{K}}^{-1}, \mathcal{I} \in \mathcal{C}$ to the processor holding $L_{\mathcal{K}, \mathcal{K}}$)
4 For the processor holding $(L_{\mathcal{K}, \mathcal{K}})^{-1}$, update
 $A_{\mathcal{K}, \mathcal{K}}^{-1} \leftarrow (U_{\mathcal{K}, \mathcal{K}})^{-1} (L_{\mathcal{K}, \mathcal{K}})^{-1} - \hat{L}_{\mathcal{C}, \mathcal{K}}^T A_{\mathcal{C}, \mathcal{K}}^{-1}$
 For the processors holding $L_{\mathcal{K}, \mathcal{K}}^{-1}$, update $A_{\mathcal{K}, \mathcal{K}}^{-1} \leftarrow \frac{1}{2} (A_{\mathcal{K}, \mathcal{K}}^{-1} + A_{\mathcal{K}, \mathcal{K}}^{-T})$
3 Overwrite $\hat{L}_{\mathcal{I}, \mathcal{K}}, \mathcal{I} \in \mathcal{C}$ by $A_{\mathcal{I}, \mathcal{K}}^{-1}, \mathcal{I} \in \mathcal{C}$
5 (Send $A_{\mathcal{I}, \mathcal{K}}^{-1}, \mathcal{I} \in \mathcal{C}$ to the processor holding $\hat{U}_{\mathcal{K}, \mathcal{I}}, \mathcal{I} \in \mathcal{C}$, and
 overwrite $\hat{U}_{\mathcal{K}, \mathcal{I}}, \mathcal{I} \in \mathcal{C}$ by $A_{\mathcal{I}, \mathcal{K}}^{-1}, \mathcal{I} \in \mathcal{C}$)

end

end

end

Problem	Description
SIESTA_C_BN_1x1	Electronic structure theory, C-BN sheet with 2532 atoms
SIESTA_C_BN_2x2	Electronic structure theory, C-BN sheet with 10128 atoms
SIESTA_C_BN_4x2	Electronic structure theory, C-BN sheet with 20256 atoms
DNA_16	Electronic structure theory, DNA molecule with 11440 atoms
DNA_715_64cell	Electronic structure theory, DNA molecule with 45760 atoms
DG_Graphene_2048	Electronic structure theory, graphene with 2048 atoms
DG_Graphene_8192	Electronic structure theory, graphene with 8192 atoms
pwtk	Pressurized wind tunnel, stiffness matrix.
parabolic_fem	Diffusion-convection reaction, constant homogeneous diffusion.
ecology2	Circuitscape: circuit theory applied to animal/gene flow, B. McRae, UCSB.
audikw_1	Automotive crankshaft model with over 900,000 TETRA elements, Audi, GmbH.

Table I: Description of test problems for PSe1Inv.

Problem	n	$ A $	$ L $
SIESTA_C_BN_1x1	32,916	23,857,418	269,760,112
SIESTA_C_BN_2x2	131,664	95,429,672	1,655,233,542
SIESTA_C_BN_4x2	263,328	190,859,344	3,591,750,262
DNA_16	7,752	2,430,642	9,272,160
DNA_715_64cell	459,712	224,055,744	866,511,698
DG_Graphene_2048	82,944	87,340,032	545,245,344
DG_Graphene_8192	331,776	349,360,128	2,973,952,468
pwtk	217,918	5,926,171	104,644,472
parabolic_fem	525,825	3,674,625	58,028,731
ecology2	999,999	2,997,995	91,073,583
audikw_1	943,695	77,651,847	2,500,489,909

Table II: The dimension n , the number of nonzeros $|A|$, and the number of nonzeros of the Cholesky factor $|L|$ of the test problems.

“symbolic factorization” in the timing figures. The LU factorization is performed by using `SuperLU_DIST`. It is labeled by “LU factorization”. The selected inversion itself is performed by using `PSe1Inv`, and labeled by “PSe1Inv”. The total time required to obtain the selected elements of the inverse matrix thus corresponds to the sum of all three components.

The first experiment focuses on the impact of the additional parallelism stemming from the elimination tree as discussed in Section 3.3. `PSe1Inv` is thus tested both with and without this additional level of parallelism. As observed in Fig. 6, adding the tree level parallelism allows the performance of `PSe1Inv` to scale to 4096 cores. When 4096 cores are used, adding the tree level parallelism leads to a 5.6 fold speedup in for the `DNA_715_64cell` problem. Comparatively, the performance of the LU factorization and the selected inversion without tree parallelism can only scale up to 1024 cores.

The second set of experiments (Figures. 7, 8 and 9) aims at evaluating the strong scaling of `PSe1Inv`. In every experiment, the tree level of parallelism is enabled as it clearly delivers better performance. `PSe1Inv` exhibits excellent strong scalability up to 4,096 cores. For SIESTA matrices (Fig. 7), `PSe1Inv` is slightly slower than LU factorization when the number of cores is less than 1024, and is faster than the LU factorization when more than 2116 cores are used. For DGDFt matrices (Fig. 8), `PSe1Inv` can be twice as fast as the LU factorization, and the running time of

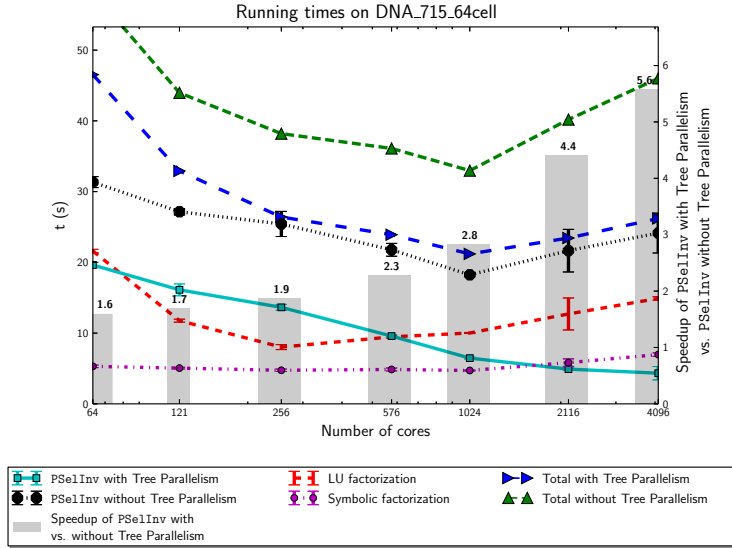


Fig. 6: The wall clock time used by three components (symbolic factorization, numerical LU factorization and selected inversion) of two versions of **PSeInv** with respect to the number of cores used in the computation for the **DNA_715_64cell** matrix. In one version, we do not take advantage of the concurrency exposed by the elimination tree, whereas in the other version we do make use of this tree level of parallelism. The height of each bar in the figure indicates the ratio of wall clocked time measured for the former over that measured for the latter.

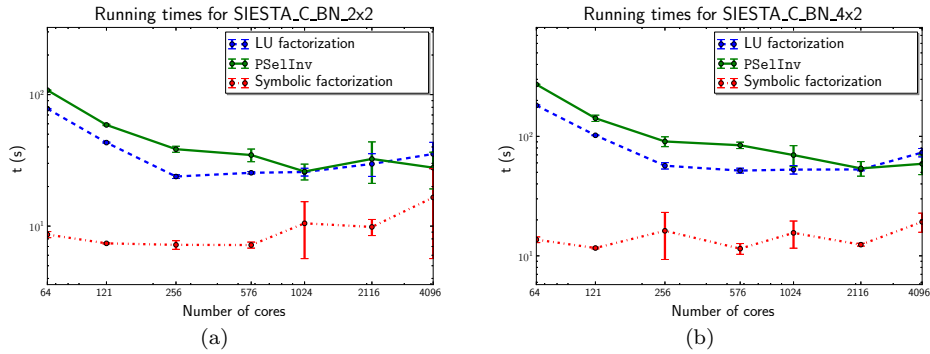


Fig. 7: The strong scalability of **PSeInv** compared to that of LU factorization and symbolic factorization for SIESTA matrices generated for two **C_BN** systems of different sizes.

PSeInv can be comparable to that of symbolic factorization for the **DNA_715_64cell** matrix. For generic sparse matrices (Fig. 9) obtained from the University of Florida Collection, **PSeInv** delivers excellent performance on relatively dense matrices, such as **audikw_1** and **pwtk**. We also observe that for highly sparse problems, such as **ecology_2** and **parabolic_fem**, **PSeInv** is relatively more costly, but the scalability of **PSeInv** can still be better than that of **SuperLU_DIST** when a large number of cores are used.

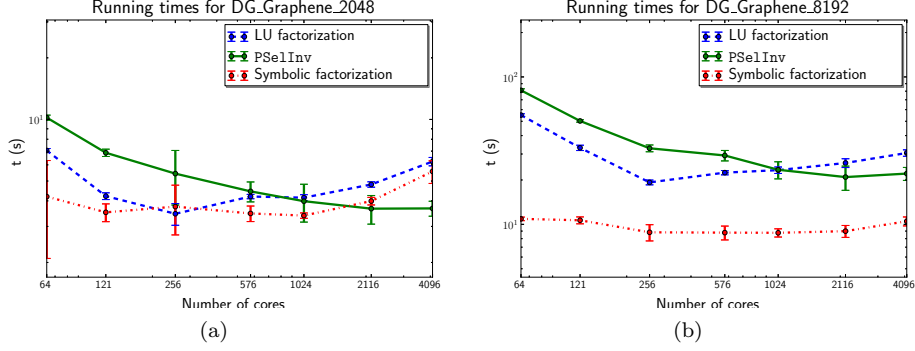


Fig. 8: The strong scalability of PSeInv compared to that of LU factorization and symbolic factorization for DG matrices generated for graphene systems of different sizes.

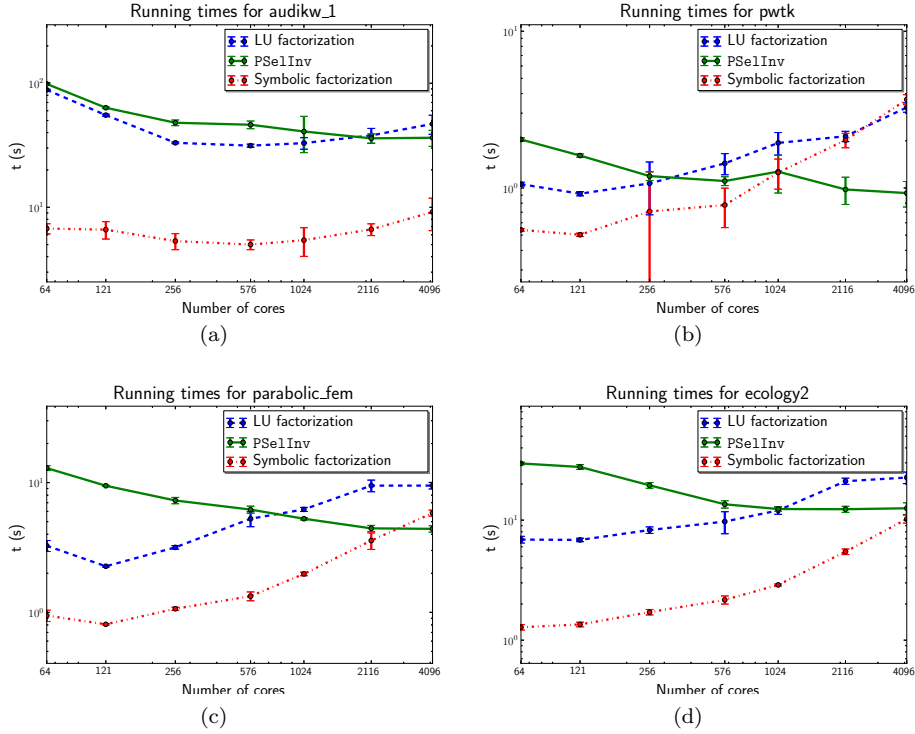


Fig. 9: The strong scalability of PSeInv compared to that of LU factorization and symbolic factorization for matrices from Harwell-Boeing Test Collection and the University of Florida Matrix Collection.

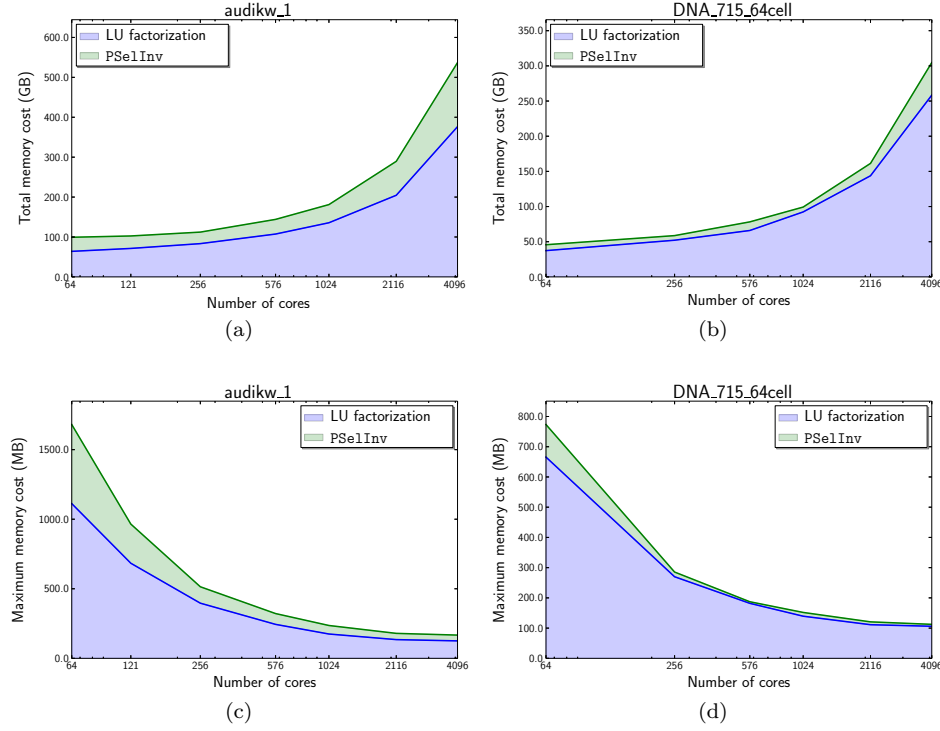


Fig. 10: The cumulative total memory cost and maximum memory cost among all cores for the `audikw_1` matrix and the `DNA_715_64cell` matrix, with shaded region indicating the additional memory cost introduced in each step of the selected inversion process. The memory cost is measured by memory high watermark reached at each step.

The third experiment focuses on the memory cost of `PSelInv`. Fig. 10 shows the cumulative total memory cost and cumulative maximum single core memory usage in the parallel selected inversion procedure for two matrices: `audikw_1` and `DNA_715_64cell`. This is measured by the memory high watermark reached after the LU factorization step and the selected inversion step, respectively. The memory cost for reading the input matrix is much smaller compared to the memory cost of LU factorization or selected inversion. The shaded areas in Fig. 10 correspond to the additional memory required to perform each step of the procedure. The memory high watermark implies that the memory cost for LU factorization not only includes the memory cost for the LU factors, but also other temporary memory allocation created during the LU factorization process. The situation is similar for the selected inversion process. The memory required to store both the LU factors and the corresponding elements in the inverse is lower than the overall memory high watermark, which accounts for additional memory required to hold communication and temporary buffers. We can see from Fig. 10, most of the memory allocation is done during the LU factorization step. The total memory cost of LU factorization and selected inversion increases as the number of cores increases due to the use of

Problem	# of cores	PSe1Inv	MUMPS
DNA_16	1	3.1	29.9
DNA_16	16	2.9	44.6
DGDFT_ACPNR4_60	1	4.9	82.6
DGDFT_ACPNR4_60	16	0.6	67.1
SIESTA_C_BN_1x1	16	52.6	648.2
SIESTA_C_BN_1x1	256	5.6	293.7

Table III: A comparison of wallclock time required by PSe1Inv and MUMPS for computing the selected elements defined by (1) of two matrices DNA_16 and SIESTA_C_BN_1x1, and the diagonal elements of DGDFT_ACPNR4_60.

additional buffer arrays for communication and computation.

The total additional memory cost of PSe1Inv is 20% ~ 60% of the total memory required by LU factorization, which is relatively small. The maximum memory usage per core decreases steadily as the number of cores increases. For our test problems, the maximum memory cost per core of PSe1Inv is around 1GB when a relatively small number (64) of cores are used. It decreases to around 100MB when a large number (4096) of cores are used for the same problem.

The last set of experiments compare the performance of PSe1Inv with the parallel matrix inversion method recently implemented in the MUMPS package [Amestoy et al. 2012]. In the MUMPS algorithm, the actual set of computed entries of A^{-1} is also a *superset* of the requested entries of A^{-1} . This method can be more efficient than PSe1Inv when a small number of entries of A^{-1} are requested. However, when a relatively large number of entries are to be computed such as in the computation of the selected elements defined by (1), PSe1Inv can more efficiently reuse the information shared among different entries of A^{-1} . Fig. 11 shows the numerical factorization and selected inversion timings for MUMPS and PSe1Inv, respectively. As all matrices are symmetric, MUMPS performs LDL^T factorizations, which use fewer floating point operations and less memory. We use MUMPS to compute the selected elements of A^{-1} as defined in Eq. (1) for DNA_16 and SIESTA_C_BN_1x1, and use MUMPS to only compute the diagonal entries of A^{-1} for DGDFT_ACPNR4_60. All three matrices come from electronic structure applications, and the difference in terms of computed entries is determined by the different requirements in practical calculations. MUMPS contains a block size parameter that controls the number of right-hand sides processed simultaneously. We experimented with this parameter, and report the best results we could produce for each case (i.e. 16 for DNA_16 and 256 for SIESTA_C_BN_1x1 and DGDFT_ACPNR4_60). Table III shows how the wallclock time used by PSe1Inv compares with that used by MUMPS for three test problems DNA_16, DGDFT_ACPNR4_60 and SIESTA_C_BN_1x1.

For all test problems, PSe1Inv is at least an order of magnitude faster than MUMPS. It is two orders of magnitude faster on SIESTA_C_BN_1x1 when using 256 cores. PSe1Inv can also scale to a relatively larger number of cores. Our numerical results indicate that for the computation of selected elements as considered in this paper, PSe1Inv is more efficient than the more general approach taken in MUMPS.

One way to understand the speedup of PSe1Inv over MUMPS is through the following idealized situation. Consider the computation of the diagonal entries of a tridiagonal matrix A of size N , which can be computed by solving N set of triangu-

lar equations of the form (5). Even with the help of the elimination tree and the fact that only one entry of A^{-1} is needed for each equation, the cost for solving all N equations independently would be $\mathcal{O}(N^2)$. The reason for the high computational cost is that a significant amount of information calculated among the N equations are redundant. The MUMPS approach is to detect such redundant information on the fly through graph based algorithms. However, designing an optimal algorithm which maximally reduces the amount of redundant information for a given data-to-processor mapping is difficult. The resulting implementation may or may not reach the optimal complexity. By contrast PSe1Inv removes all the redundant calculation *by design*, and the computational cost for a tri-diagonal matrix can be provably reduced to $\mathcal{O}(N)$ [Lin et al. 2009b].

We should point out that MUMPS can compute an arbitrary set of elements of A^{-1} , whereas the set of selected elements that can be computed by PSe1Inv is more restrictive as defined in Eq. (1).

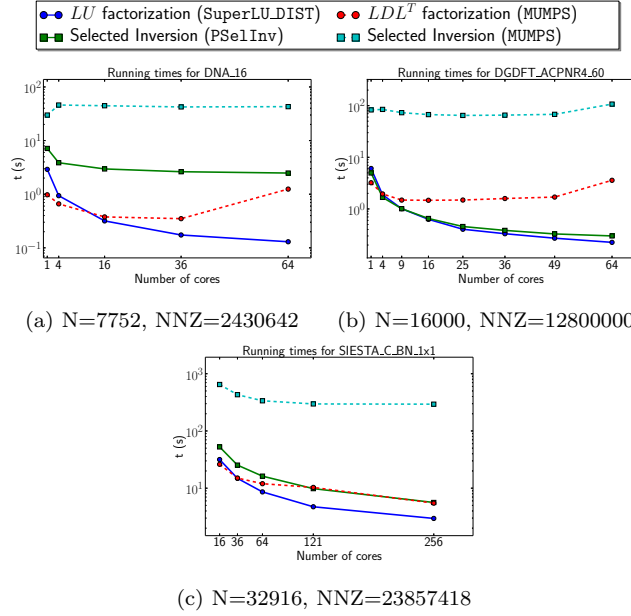


Fig. 11: Performance comparison against MUMPS 4.10.0 for computing selected elements of the inverse.

Overall, the strong scalability of PSe1Inv is similar to that of SuperLU-DIST and it clearly outperforms current inversion algorithm as implemented in MUMPS. It requires a modest amount of additional memory to compute the selected elements of the inverse. This observation demonstrates both the validity of our approach and the efficiency of our implementation. More importantly, on matrices arising from actual electronic calculations, PSe1Inv allows one to use thousands of cores, thereby enabling very large-scale computations.

P	Max. relative error	P	Max. relative error
1	8.52E-008	16	1.96E-007
4	2.35E-008	36	1.72E-007
16	2.52E-008	64	1.77E-007
36	2.05E-007	121	1.76E-007
64	2.07E-007	256	1.78E-007

(a) DNA_16
(b) SIESTA_C.BN_1x1

Table IV: Maximum column-wise relative error between **MUMPS** and **PSelInv** using different number of cores P .

4.2 The Accuracy of **PSelInv**

In exact arithmetic, the selected inversion method is an exact method for computing the selected elements of A^{-1} , regardless of whether A is positive definite or not. In practice, the selected inversion method cannot give an exact result due to the presence of round off errors. For sparse direct solver, dynamical pivoting strategies such as the Bunch-Kaufman process [Bunch and Kaufman 1977] for LDL^T factorization has been shown to be effective for reducing the numerical error especially for indefinite matrices. On distributed memory machines, dynamic pivoting strategies can significantly affect the load balance and the scalability of the factorization process. Thus, they are not used in **SuperLU_DIST** [Li and Demmel 2003].

Since the primary goal of the current implementation of the **PSelInv** method is to achieve high parallel scalability, we choose not to perform additional pivoting steps after the factorization step. We show that for the test problems we tried, **PSelInv** produces results comparable to that produced by the **MUMPS** package, and is sufficiently accurate even when the matrix is relatively ill conditioned.

The first set of experiments reports comparative results between **MUMPS** and **PSelInv** on two problems benchmarked in Section 4.1. Selected elements are computed with both methods and their maximum relative column-wise difference $\max_{1 \leq j \leq n} (\|A_{\text{MUMPS},*,j}^{-1} - A_{\text{PSelInv},*,j}^{-1}\| / \|A_{\text{MUMPS},*,j}^{-1}\|)$ is presented in Table IV. In both cases, **PSelInv** provides accurate results which are comparable to **MUMPS** on these two problems.

In the second set of experiments, we assess the accuracy of **PSelInv** on larger ill conditioned matrices. To obtain test problems that are indefinite and ill conditioned, for each test problem listed in Tab. II, we construct a sequence of $A(z)$ defined by Eq. (18) for a number of complex shifts z . The real parts of the shifts lie within the spectrum of the matrix pencil (H, S) , and the imaginary parts range from small (10^{-7}) to large (10^{-1}) values.

In order to quantify the accuracy of the **PSelInv** method for large matrices in the test set, we need to find an appropriate error metric. Due to the large matrix size, the parallel matrix inversion method in **MUMPS** becomes too expensive to be used for the purpose of benchmarking. Motivated by the trace estimation in Eq. (2), we choose to measure the numerical error introduced by **PSelInv** by using the following

quantity

$$E(z) = \frac{|N - \text{Tr}[A(z)^{-1}A(z)]|}{N} \equiv \left| 1 - \frac{1}{N} \sum_{i,j=1}^N [A(z)^{-1}]_{ij}[A(z)]_{ji} \right|. \quad (19)$$

Since A is sparse, the summation in Eq. (19) involves only those i and j such that $A_{i,j} \neq 0$.

In Fig. 12, we show both the spectral density $\rho(\lambda)$ of the pwtk matrix, which describes the number of eigenvalues of eigenvalues (H, S) per unit interval, and $E(z)$ for a number of shifts z with different real and imaginary parts. We observe that for all these problems, the measured errors are below 10^{-11} , even when the real part of z is close to an eigenvalue cluster and the imaginary part of z is as small as 10^{-7} . Fig. 13 shows that a similar level of accuracy is achieved in the test of DNA_715_64cell matrix.

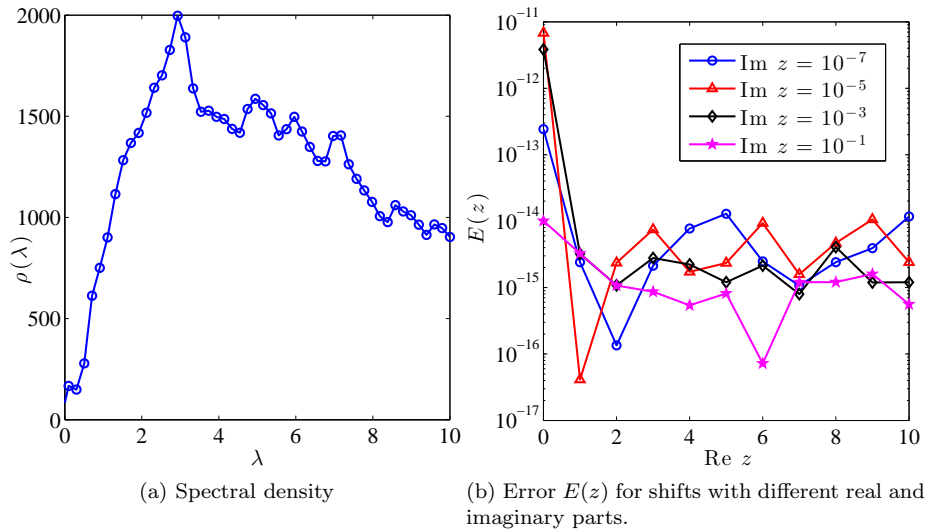
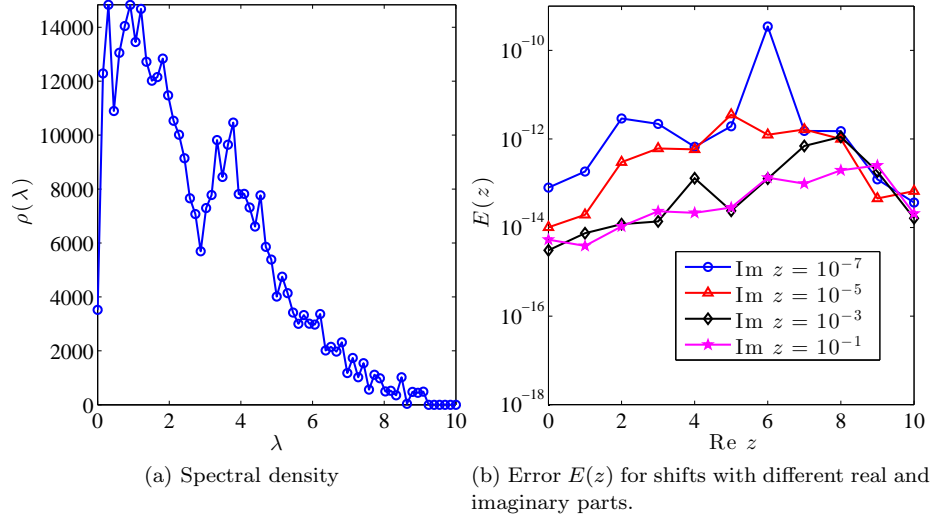


Fig. 12: Spectral density and error $E(z)$ for the pwtk matrix.

4.3 Application to electronic structure theory

In this section, we demonstrate how PSelInv can be applied to accelerate Kohn-Sham density functional theory (KSDF) calculation [Hohenberg and Kohn 1964; Kohn and Sham 1965], which is widely used for describing the ground state electronic properties of molecules, solids and other nano structures. We use the recently developed pole expansion and selected inversion technique (PEXSI) [Lin et al. 2009a; 2009b; 2011b; 2013] to compute the non-zero elements of the so-called

Fig. 13: Spectral density and error $E(z)$ for the DNA_715_64cell matrix.

single particle density matrix Γ that can be approximated by

$$\Gamma \approx \sum_{l=1}^P \omega_l (H - z_l S)^{-1}. \quad (20)$$

where $z_l, \omega_l \in \mathbb{C}$, and the number of “poles” P is around 80 in practical calculations. Both H and S are real sparse symmetric matrices that have the same sparsity pattern when a local basis set is used to discretize the Kohn-Sham problem. Each matrix $A_l = H - z_l S$ is a complex symmetric matrix. In KSDFT calculations, only elements of Γ_{ij} corresponding to the nonzero elements of H and S (i.e. $H_{ij}, S_{ij} \neq 0$) are needed to compute physical quantities such as electron density and energy. The expansion (20) immediately suggests that only the selected elements as defined in Eq. (1) of the matrices A_l^{-1} are needed. In a parallel implementation of PEXSI, we use `PSeInv` to evaluate the selected elements of A_l^{-1} that correspond to the nonzero elements of Γ on a subset of cores. The selected inversion of A_l for different l can be carried out independently on different subsets of cores.

We apply the parallel PEXSI method to the DG_Graphene_2048 and DG_Graphene_8192 systems, which are disordered graphene systems with 2048 and 8192 atoms, respectively, and compare its performance with a standard approach that requires a partial diagonalization of (H, S) . We use a ScaLAPACK subroutine `pdsyevr` [Vömel 2010], which is based on the multiple relatively robust representations (MRRR) algorithm, to perform such diagonalization. Though both H and S are sparse matrices, the MRRR algorithm treats them as dense matrices. For $H, S \in \mathbb{R}^{N \times N}$, the MRRR algorithm first performs a tridiagonalization procedure with $\mathcal{O}(N^3)$ cost, then efficiently solves the eigenvalues and eigenvectors of the tridiagonal system with $\mathcal{O}(N^2)$ cost, and finally the eigenvectors can be constructed with $\mathcal{O}(N^3)$ cost.

Fig. 14(a) shows that the scalability of `pdsyevr` is limited to 1024 cores for the 2048-atom problem. Adding more cores to the diagonalization process leads to an increase of the wall clock time due to communication overhead. For this relatively small problem, the benefit of parallel implementation of PEXSI is already clear when 320 cores are used. Since we use $P = 80$ poles in the pole expansion, 4 cores with a 2×2 processor grid are used in each selected inversion in this case. The wall clock time used by PEXSI is 261 seconds, among which 150 seconds are attributed to `PSe1Inv`, 95 seconds are attributed to factorization, and 10 seconds for symbolic factorization. This timing result compares favorably to the 430 seconds of measured wall clock time required by `pdsyevr` on 1,024 cores.

Furthermore, we can clearly see from Fig. 14(a) that the parallel PEXSI method can scale to a much larger number of cores. Nearly perfect speedup can be observed when a total of 20,480 cores are used in the parallel PEXSI computation, with 256 cores used in each selected inversion. The total wall clock time used in this calculation is merely 10 seconds. Compared to the best wall clock time we can obtain for the diagonalization procedure, which is 430 sec on 1,024 cores, this represents a speedup factor of 43.

For the larger system that contains 8192 atoms, `pdsyevr` can scale to 4,096 cores as we can see in Fig. 14(b). It takes 5703 wall clock seconds to perform such a computation. When the parallel PEXSI calculation is carried out on 5,120 cores with 64 cores used to perform each selected inversion, the total wall clock time required is 224 seconds. Fig. 14(b) also shows that parallel PEXSI can scale to as many as 327,680 cores with 4,096 cores used for each selected inversion. The total wallclock time required in this calculation is merely 45 seconds, a 127 fold speedup compared to the best diagonalization wallclock time measured.

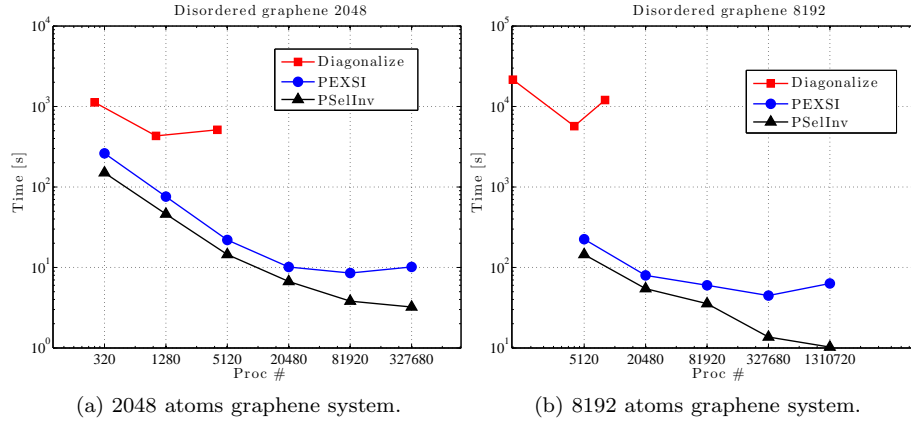


Fig. 14: The wall clock time versus the number of cores for a graphene system.

Finally we apply PEXSI to a system with 32,768 atoms. The matrix size is 4 times larger than that for the system with 8,192 atoms, and the diagonalization routine is no longer feasible: the wall clock time required to run `pdsyevr` routine

with 1024 cores for the 2048-atom system is 431 sec, and for the 8192-atom system is 21556 sec. The increase of the wall clock time is 50 fold, which is roughly in agreement with the cubic complexity scaling factor $4^3 = 64$. The cubic scaling of the diagonalization procedure implies that the wall clock time would increase by at least a factor of 50 to 1,077,800 seconds (300 hours) if we perform the same type of calculation for a system that contains 32,768 atoms on 1,024 cores. Based on this estimation and assuming that the strong scaling of `pdsyevr` is perfect, we compare the ideal performance of the diagonalization method with the practical performance of PEXSI in Fig. 15 up to 1,310,720 cores. The total wall clock time for both factorization and selected inversion reaches its minimum at 4,096 cores per pole (327,680 cores in total), which is 241 sec. Among these, 87 sec is attributed to `PSelInv`. Comparatively, even if the diagonalization procedure scales perfectly to more than 1 million cores, which is highly unlikely within the current framework of diagonalization methods, the projected wall clock time is over 1000 sec, which is significantly more than that used by PEXSI.

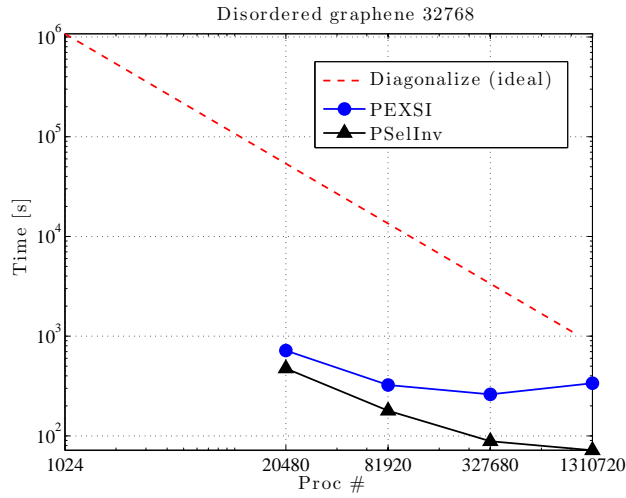


Fig. 15: The wall clock time versus the number of cores for a graphene system with 32768 atoms.

5. CONCLUSION AND FUTURE WORK

We described an efficient parallel implementation of the selected inversion algorithm for distributed memory parallel machines. The current implementation of `PSelInv` can be applied to the computation of selected elements of the inverse of a sparse symmetric matrix. It is publicly available, and can scale to more than 4000 cores for sufficiently large problems. The scalability of the solver depends on the size and sparsity of the matrix. We observed that it is important to exploit concurrency available within the elimination trees to achieve high scalability in the parallel selected inversion process. In the future, we plan to further improve the tree level parallelism to enhance the concurrency among different supernodes. We

also observed that, for our test problems, the PSeInv method is relatively accurate even for matrices that are highly indefinite and close to singular. It can be applied to accelerate several scientific computation applications such as the density functional theory based electronic structure calculations. In order to further improve the numerical accuracy of the PSeInv method, especially for indefinite matrices, dynamic pivoting strategies such as Bunch-Kaufman procedure [Bunch and Kaufman 1977; Grimes et al. 1994] for the factorization may be needed. Generalizing PSeInv to non-symmetric matrices and combining it with other sparse direct solvers are also areas we plan to work on in the future.

ACKNOWLEDGMENTS

This work was partially supported by the Laboratory Directed Research and Development Program of Lawrence Berkeley National Laboratory under the U.S. Department of Energy contract number DE-AC02-05CH11231 (L. L. and C. Y.), the Scientific Discovery through Advanced Computing (SciDAC) program funded by U.S. Department of Energy, Office of Science, Advanced Scientific Computing Research and Basic Energy Sciences (M. J., L. L. and C. Y.), and the Center for Applied Mathematics for Energy Research Applications (CAMERA), which is a partnership between Basic Energy Sciences (BES) and Advanced Scientific Computing Research (ASRC) at the U.S Department of Energy. We would like to thank Xiaoye S. Li and François-Henry Rouet for helpful discussion.

REFERENCES

- AMESTOY, P., DUFF, I., L'EXCELLENT, J.-Y., AND KOSTER, J. 2001. A fully asynchronous multifrontal solver using distributed dynamic scheduling. *SIAM J. Matrix Anal. and Appl.* **23**, 15–41.
- AMESTOY, P. R., DUFF, I. S., L'EXCELLENT, J.-Y., ROBERT, Y., ROUET, F.-H., AND UÇAR, B. 2012. On computing inverse entries of a sparse matrix in an out-of-core environment. *SIAM J. Sci. Comput.* **34**, A1975–A1999.
- AMESTOY, P. R., DUFF, I. S., L'EXCELLENT, J. Y., AND ROUET, F. H. 2012. Parallel computation of entries of A^{-1} . Tech. rep., CERFACS, Toulouse, France.
- ASHCRAFT, C. AND GRIMES, R. 1989. The influence of relaxed supernode partitions on the multifrontal method. *ACM Trans. Math. Software* **15**, 291–309.
- BEKAS, C., CURIONI, A., AND FEDULOVA, I. 2009. Low cost high performance uncertainty quantification. In *Proc. 2nd Workshop on High Performance Computational Finance*. 8.
- BEKAS, C., KOKIOPOULOU, E., AND SAAD, Y. 2007. An estimator for the diagonal of a matrix. *Appl. Numer. Math.* **57**, 1214–1229.
- BLACKFORD, L. S. 1997. *ScaLAPACK user's guide*. Vol. 4. SIAM.
- BUNCH, J. R. AND KAUFMAN, L. 1977. Some stable methods for calculating inertia and solving symmetric linear systems. *Math. Comp.*, 163–179.
- CAMPBELL, Y. E. AND DAVIS, T. A. 1995. Computing the sparse inverse subset: an inverse multifrontal approach. Tech. Rep. TR-95-021, University of Florida.
- CAULEY, S., BALAKRISHNAN, V., KLIMECK, G., AND KOH, C.-K. 2012. A two-dimensional domain decomposition technique for the simulation of quantum-scale devices. *J. Comput. Phys.* **231**, 4, 1293–1313.
- CHEVALIER, C. AND PELLEGRINI, F. 2008. PT-Scotch: A tool for efficient parallel graph ordering. *Parallel Comput.* **34**, 318–331.
- DAVIS, T. A. AND HU, Y. 2011. The University of Florida sparse matrix collection. *ACM Trans. Math. Software* **38**, 1.

- DUFF, I., GRIMES, R., AND LEWIS, J. 1992. User's guide for the Harwell-Boeing sparse matrix collection. *Research and Technology Division, Boeing Computer Services, Seattle, Washington, USA*.
- EASTWOOD, S. AND WAN, J. 2013. Finding off-diagonal entries of the inverse of a large symmetric sparse matrix. *Numer. Linear Algebra Appl.* 20, 1, 74–92.
- ERISMAN, A. AND TINNEY, W. 1975. On computing certain elements of the inverse of a sparse matrix. *Comm. ACM* 18, 177.
- GOLUB, G. H. AND VAN LOAN, C. F. 1996. *Matrix computations*, third ed. Johns Hopkins Univ. Press, Baltimore.
- GRIMES, R. G., LEWIS, J. G., AND SIMON, H. D. 1994. A shifted block Lanczos algorithm for solving sparse symmetric generalized eigenproblems. *SIAM Journal on Matrix Analysis and Applications* 15, 1 (January), 228–272.
- HETMANIUK, U., ZHAO, Y., AND ANANTRAM, M. P. 2013. A nested dissection approach to modeling transport in nanodevices: Algorithms and applications. *Int. J. Numer. Meth. Eng.*
- HOHENBERG, P. AND KOHN, W. 1964. Inhomogeneous electron gas. *Phys. Rev.* 136, B864–B871.
- JACQUELIN, M., LIN, L., AND YANG, C. 2014. PSELInv—a distributed memory parallel algorithm for selected inversion: the symmetric case. Tech. rep.
- KARYPIS, G. AND KUMAR, V. 1998. A parallel algorithm for multilevel graph partitioning and sparse matrix ordering. *J. Parallel Distrib. Comput.* 48, 71–85.
- KOHN, W. AND SHAM, L. 1965. Self-consistent equations including exchange and correlation effects. *Phys. Rev.* 140, A1133–A1138.
- KOTLIAR, G., SAVRASOV, S. Y., HAULE, K., OUDOVENKO, V. S., PARCOLLET, O., AND MARIANETTI, C. 2006. Electronic structure calculations with dynamical mean-field theory. *Rev. Mod. Phys.* 78, 865–952.
- KUZMIN, A., LUISIER, M., AND SCHENK, O. 2013. Fast methods for computing selected elements of the Greens function in massively parallel nanoelectronic device simulations. In *Euro-Par 2013 Parallel Processing*. Springer, 533–544.
- LANCZOS, C. 1950. An iteration method for the solution of the eigenvalue problem of linear differential and integral operators. *J. Res. Nat. Bur. Stand.* 45, 255–282.
- LI, S., AHMED, S., KLIMECK, G., AND DARVE, E. 2008. Computing entries of the inverse of a sparse matrix using the FIND algorithm. *J. Comput. Phys.* 227, 9408–9427.
- LI, S. AND DARVE, E. 2012. Extension and optimization of the find algorithm: Computing greens and less-than greens functions. *Journal of Computational Physics* 231, 4, 1121–1139.
- LI, S., WU, W., AND DARVE, E. 2013. A fast algorithm for sparse matrix computations related to inversion. *J. Comput. Phys.* 242, 915–945.
- LI, X. S. AND DEMMEL, J. W. 2003. SuperLU-DIST: A scalable distributed-memory sparse direct solver for unsymmetric linear systems. *ACM Trans. Math. Software* 29, 110.
- LIN, L., CHEN, M., YANG, C., AND HE, L. 2013. Accelerating atomic orbital-based electronic structure calculation via pole expansion and selected inversion. *J. Phys. Condens. Matter* 25, 295501.
- LIN, L., LU, J., YING, L., CAR, R., AND E, W. 2009b. Fast algorithm for extracting the diagonal of the inverse matrix with application to the electronic structure analysis of metallic systems. *Comm. Math. Sci.* 7, 755.
- LIN, L., LU, J., YING, L., AND E, W. 2009a. Pole-based approximation of the Fermi-Dirac function. *Chin. Ann. Math.* 30B, 729.
- LIN, L., LU, J., YING, L., AND E, W. 2012. Adaptive local basis set for Kohn-Sham density functional theory in a discontinuous Galerkin framework I: Total energy calculation. *J. Comput. Phys.* 231, 2140–2154.
- LIN, L., YANG, C., LU, J., YING, L., AND E, W. 2011a. A fast parallel algorithm for selected inversion of structured sparse matrices with application to 2D electronic structure calculations. *SIAM J. Sci. Comput.* 33, 1329.
- LIN, L., YANG, C., MEZA, J., LU, J., YING, L., AND E, W. 2011b. SelInv – An algorithm for selected inversion of a sparse symmetric matrix. *ACM. Trans. Math. Software* 37, 40.

- LIU, J. 1990. The role of elimination trees in sparse factorization. *SIAM J. Matrix Anal. Appl.* 11, 134.
- PETERSEN, D. E., LI, S., STOKBRO, K., SØRENSEN, H. H. B., HANSEN, P. C., SKELBOE, S., AND DARVE, E. 2009. A hybrid method for the parallel computation of Green's functions. *J. Comput. Phys.* 228, 5020–5039.
- ROTHBERG, E. AND GUPTA, A. 1994. An efficient block-oriented approach to parallel sparse Cholesky factorization. *SIAM J. Sci. Comput.* 15, 1413–1439.
- SCHENK, O. AND GARTNER, K. 2006. On fast factorization pivoting methods for symmetric indefinite systems. *Elec. Trans. Numer. Anal.* 23, 158–179.
- SIDJE, R. B. AND SAAD, Y. 2011. Rational approximation to the Fermi-Dirac function with applications in density functional theory. *Numer. Algor.* 56, 455.
- SOLER, J. M., ARTACHO, E., GALE, J. D., GARCÍA, A., JUNQUERA, J., ORDEJÓN, P., AND SÁNCHEZ-PORTAL, D. 2002. The SIESTA method for ab initio order-N materials simulation. *J. Phys.: Condens. Matter* 14, 2745–2779.
- TAKAHASHI, K., FAGAN, J., AND CHIN, M. 1973. Formation of a sparse bus impedance matrix and its application to short circuit study. In *8th PICA Conf. Proc.*
- TANG, J. M. AND SAAD, Y. 2012. A probing method for computing the diagonal of a matrix inverse. *Numer. Lin. Alg. Appl.* 19, 485–501.
- VÖMEL, C. 2010. ScaLAPACK's MRRR algorithm. *ACM Trans. Math. Software* 37, 1.
- XU, Z. AND MAGGS, A. C. 2013. Solving fluctuation-enhanced Poisson-Boltzmann equations. *arXiv:1310.4682*.